Nonzero orbital angular momentum superfluidity in ultracold Fermi gases

M. Iskin and C. A. R. Sá de Melo
School of Physics, Georgia Institute of Technology, Atlanta, Georgia 30332, USA
(Received 6 February 2006; revised manuscript received 18 April 2006; published 13 July 2006)

We analyze the evolution of superfluidity for nonzero orbital angular momentum channels from the Bardeen-Cooper-Schrieffer (BCS) to the Bose-Einstein condensation (BEC) limit in three dimensions. First, we analyze the low-energy scattering properties of finite range interactions for all possible angular momentum channels. Second, we discuss ground-state ($T=0$) superfluid properties including the order parameter, chemical potential, quasiparticle excitation spectrum, momentum distribution, atomic compressibility, ground-state energy, and low-energy collective excitations. We show that a quantum phase transition occurs for nonzero angular momentum pairing, unlike the s-wave case where the BCS to BEC evolution is just a crossover. Third, we present a Gaussian fluctuation theory near the critical temperature ($T=T_c$), and we analyze the number of bound, scattering, and unbound fermions as well as the chemical potential. Finally, we derive the time-dependent Ginzburg-Landau functional near T_c, and compare the Ginzburg-Landau coherence length with the zero-temperature average Cooper pair size.

DOI: 10.1103/PhysRevA.74.013608 PACS number(s): 03.75.Ss, 03.75.Hh, 74.25.Bt, 74.25.Dw

I. INTRODUCTION

Experimental advances involving atomic Fermi gases enabled the control of interactions between atoms in different hyperfine states by using Feshbach resonances [1–7]. These resonances can be tuned via an external magnetic field and allow the study of dilute many-body systems with fixed density, but varying interaction strength characterized by the scattering parameter a_ℓ. This technique allows for the study of new phases of strongly interacting fermions. For instance, the recent experiments from the MIT group [8] marked the first observation of vortices in atomic Fermi gases corresponding to a strong signature of superfluidity in the s-wave ($\ell=0$) channel. These studies combined [1–8] correspond to the experimental realization of the theoretically proposed Bardeen-Cooper-Schrieffer (BCS) to Bose-Einstein condensation (BEC) crossover [9–13] in three-dimensional (3D) s-wave superfluids. Recent extensions of these ideas include trapped fermions [14,15] and fermion-boson models [16–18].

Arguably one of the next frontiers of exploration in ultracold Fermi systems is the search for superfluidity in higher angular momentum states ($\ell\neq 0$). Substantial experimental progress has been made recently [19–23] in connection to p-wave ($\ell=1$) cold Fermi gases, making them ideal candidates for the observation of novel triplet superfluid phases. These phases may be present not only in atomic, but also in nuclear (pairing in nuclei), astrophysics (neutron stars), and condensed-matter (organic superconductors) systems.

The tuning of p-wave interactions in ultracold Fermi gases was initially explored via p-wave Feshbach resonances in trap geometries for ^{40}K in Refs. [19,20] and ^{6}Li in Refs. [21,22]. Finding and sweeping through these resonances is difficult since they are much narrower than the s-wave case, because atoms interacting via higher angular momentum channels have to tunnel through a centrifugal barrier to couple to the bound state [20]. Furthermore, while losses due to two body dipolar [21,24] or three-body [19,20] processes challenged earlier p-wave experiments, these losses were still present but were less dramatic in the very recent optical lattice experiment involving ^{40}K and p-wave Feshbach resonances [23].

Furthermore, due to the magnetic dipole-dipole interaction between valence electrons of alkali atoms, the nonzero angular momentum Feshbach resonances corresponding to projections of angular momentum ℓ $[m_\ell=\pm\ell,\pm(\ell-1),\ldots,0]$ are nondegenerate (separated from each other) with total number of $\ell+1$ resonances [20]. Therefore, in principle, these resonances can be tuned and studied independently if the separation between them is larger than the experimental resolution. Since the ground state is highly dependent on the separation and detuning of these resonances, it is possible that p-wave superfluid phases can be studied from the BCS to the BEC regime. For sufficiently large splittings, it has been proposed [25,26] that pairing occurs only in $m_\ell=0$ and does not occur in the $m_\ell=\pm 1$ states. However, for small splittings, pairing occurs via a linear combination of the $m_\ell=0$ and $m_\ell=\pm 1$ states. Thus the $m_\ell=0$ or $m_\ell=\pm 1$ resonances may be tuned and studied independently if the splitting is large enough in comparison to the experimental resolution.

The BCS to BEC evolution of d-wave ($\ell=2$) superfluidity was discussed previously in the literature using continuum [27–29] and lattice [30,31] descriptions in connection to high-T_c superconductivity. More recently, p-wave superfluidity was analyzed at $T=0$ for two hyperfine state (THS) systems in three dimensions [32], and for single hyperfine state (SHS) systems in two dimensions [33–35], using fermion-only models. Furthermore, fermion-boson models were proposed to describe p-wave superfluidity at zero [25,26] and finite temperature [36] in three dimensions. In this manuscript, we present a generalization of the zero and finite temperature analysis of both THS pseudospin singlet and SHS pseudospin triplet [37] superfluidity in three dimensions within a fermion-only description.

The rest of the paper is organized as follows. In Sec. II, we analyze the interaction potential in both real and momentum space for nonzero orbital momentum channels. We in-

troduce the imaginary-time functional integration formalism in Sec. III, and obtain the self-consistency (order parameter and number) equations. There we also discuss the low-energy scattering amplitude of a finite range interaction for all possible angular momentum channels, and relate the self-consistency equations to scattering parameters. In Sec. IV, we discuss the evolution from BCS to BEC superfluidity at zero temperature. There we analyze the order parameter, chemical potential, quasiparticle excitation spectrum, momentum distribution, atomic compressibility, and ground-state energy as a function of scattering parameters. We also discuss Gaussian fluctuations and low-energy collective excitations at zero temperature in Sec. V. In Sec VI, we present the evolution of superfluidity from the BCS to the BEC regimes near the critical temperature. There we discuss the importance of Gaussian fluctuations, and analyze the number of unbound, scattering, and bound fermions, critical temperature, and chemical potential as a function of scattering parameters. In Sec. VII, we derive time-dependent Ginzburg-Landau (TDGL) equation and extract the Ginzburg-Landau (GL) coherence length and time. There, we recover the GL equation in the BCS and the GP equation in the BEC limit. A short summary of our conclusions is given in Sec. VIII. Finally, we present in Appendixes A and B the coefficients for the low-frequency and long-wavelength expansion of the action at zero and finite temperatures, respectively.

II. GENERALIZED HAMILTONIAN

The Hamiltonian for a dilute Fermi gas is given by

$$H = \sum_{\mathbf{k},s_1} \xi(\mathbf{k}) a^\dagger_{\mathbf{k},s_1} a_{\mathbf{k},s_1} + \frac{1}{2\mathcal{V}} \times \sum_{\mathbf{k},\mathbf{k}',\mathbf{q}} \sum_{s_1,s_2,s_3,s_4} V^{s_3,s_4}_{s_1,s_2}(\mathbf{k},\mathbf{k}') b^\dagger_{s_1,s_2}(\mathbf{k},\mathbf{q}) b_{s_3,s_4}(\mathbf{k}',\mathbf{q}), \tag{1}$$

where s_n labels the pseudospins corresponding to trapped hyperfine states and $\mathcal{V}$ is the volume. These states are represented by the creation operator $a^\dagger_{\mathbf{k},s_1}$, and $b^\dagger_{s_1,s_2}(\mathbf{k},\mathbf{q}) = a^\dagger_{\mathbf{k}+\mathbf{q}/2,s_1} a^\dagger_{-\mathbf{k}+\mathbf{q}/2,s_2}$. Here, $\xi(\mathbf{k}) = \epsilon(\mathbf{k}) - \mu$ where $\epsilon(\mathbf{k}) = k^2/(2M)$ is the energy and μ is the chemical potential of fermions.

The interaction term can be written in a separable form $V^{s_3,s_4}_{s_1,s_2}(\mathbf{k},\mathbf{k}') = \Gamma^{s_3,s_4}_{s_1,s_2} V(\mathbf{k},\mathbf{k}')$, where $\Gamma^{s_3,s_4}_{s_1,s_2}$ is the spin and $V(\mathbf{k},\mathbf{k}')$ is the spatial part, respectively. In the case of THS case, where $s_n \equiv (\uparrow,\downarrow)$, both pseudospin singlet and pseudospin triplet pairings are allowed. However, we concentrate on the pseudospin singlet THS state with $\Gamma^{s_3,s_4}_{s_1,s_2} = \Gamma^{s_3,s_4}_{s_1,s_2} \delta_{s_1,-s_2} \delta_{s_2,s_3} \delta_{s_3,-s_4}$. In addition, we discuss the SHS case ($s_n \equiv \uparrow$), where only pseudospin triplet pairing is allowed, and the interaction is given by $\Gamma^{s_3,s_4}_{s_1,s_2} = \Gamma^{s_3,s_4}_{s_1,s_2} \delta_{s_1,s_2} \delta_{s_2,s_3} \delta_{s_3,s_4} \delta_{s_4,\uparrow}$. In this manuscript, we analyze THS singlet and SHS triplet cases for all allowable angular momentum channels. THS triplet pairing is more involved due to the more complex nature of the vector order parameters, and therefore we postpone this discussion for a future paper.

The two fermion interaction can be expanded as

$$V(\mathbf{k},\mathbf{k}') = 4\pi \sum_{\ell,m_\ell} V_\ell(k,k') Y_{\ell,m_\ell}(\hat{\mathbf{k}}) Y^*_{\ell,m_\ell}(\hat{\mathbf{k}}'), \tag{2}$$

where $Y_{\ell,m_\ell}(\hat{\mathbf{k}})$ is the spherical harmonic of order (ℓ,m_ℓ), $\Sigma_{\ell,m_\ell} = \Sigma_{\ell=0}^{\infty} \Sigma_{m_\ell=-\ell}^{\ell}$, and $\hat{\mathbf{k}}$ denotes the angular dependence $(\theta_{\mathbf{k}},\phi_{\mathbf{k}})$. The interaction should have the necessary symmetry under the Parity operation, where the transformation $\mathbf{k} \to -\mathbf{k}$ or $\mathbf{k}' \to -\mathbf{k}'$ leads to $V(\mathbf{k},\mathbf{k}')$ for singlet, and $-V(\mathbf{k},\mathbf{k}')$ for triplet pairing. Furthermore, $V(\mathbf{k},\mathbf{k}')$ is invariant under the transformation $(\mathbf{k},\mathbf{k}') \to (-\mathbf{k},-\mathbf{k}')$, and $V(\mathbf{k},\mathbf{k}')$ reflects the Pauli exclusion principle. The (k,k') dependent coefficients $V_\ell(k,k')$ are related to the real-space potential $V(r)$ through the relation $V_\ell(k,k') = 4\pi \int_0^\infty dr r^2 j_\ell(kr) j_\ell(k'r) V(r)$, where $j_\ell(kr)$ is the spherical Bessel function of order ℓ. The index ℓ labels angular momentum states in three dimensions, with $\ell = 0,1,2,\ldots$ corresponding to $s,p,d,\ldots$ channels, respectively.

Under these circumstances, we choose to study a model potential that contains most of the features described above. One possibility is to retain only one of the ℓ terms in Eq. (2), by assuming that the dominant contribution to the scattering process between Fermionic atoms occurs in the ℓth angular momentum channel. This assumption may be experimentally relevant since atom-atom dipole interactions split different angular momentum channels such that they may be tuned independently. Using the properties discussed above, we write

$$V_\ell(k,k') = -\lambda_\ell \Gamma_\ell(k) \Gamma_\ell(k'), \tag{3}$$

where $\lambda_\ell > 0$ is the interaction strength, and the function

$$\Gamma_\ell(k) = \frac{(k/k_0)^\ell}{(1 + k^2/k_0^2)^{(\ell+1)/2}} \tag{4}$$

describes the momentum dependence. Here, $k_0 \sim R_0^{-1}$ plays the role of the interaction range in real space and sets the scale at small and large momenta. In addition, the diluteness condition $(n_\ell R_0^3 \ll 1)$ requires $(k_0/k_F)^3 \gg 1$, where n_ℓ is the density of atoms and k_F is the Fermi momentum. This function reduces to $\Gamma_\ell(k) \sim k^\ell$ for small k, and behaves as $\Gamma_\ell(k) \sim 1/k$ for large k, which guarantees the correct qualitative behavior expected for $V_\ell(k,k')$ according to the analysis above.

III. FUNCTIONAL INTEGRAL FORMALISM

In this section, we describe in detail the THS singlet case for even angular momentum states. A similar approach for the SHS triplet case for odd angular momentum states can be found in Ref. [34], and therefore we do not repeat the same analysis here. However, we point out the main differences between the two cases whenever it is necessary.

A. THS singlet effective action

In the imaginary-time functional integration formalism ($\hbar = k_B = 1$ and $\beta = 1/T$), the partition function for the THS

singlet case can be written as $Z_\ell = \int D(a^\dagger, a) e^{-S_\ell}$ with action $S_\ell = \int_0^\beta d\tau [\Sigma_{\mathbf{k},s} a^\dagger_{\mathbf{k},s}(\tau)(\partial_\tau) a_{\mathbf{k},s}(\tau) + H_\ell(\tau)]$ where the Hamiltonian for the ℓth angular momentum channel is $H_\ell(\tau) = \Sigma_{\mathbf{k},s} \xi_\ell(\mathbf{k}) a^\dagger_{\mathbf{k},s}(\tau) a_{\mathbf{k},s}(\tau) - \frac{4\pi\lambda_\ell}{\mathcal{V}} \Sigma_{\mathbf{q},m_\ell} b^\dagger_{\ell,m_\ell}(\mathbf{q},\tau) b_{\ell,m_\ell}(\mathbf{q},\tau)$. Here, $b_{\ell,m_\ell}(\mathbf{q},\tau) = \Sigma_{\mathbf{k}} \Gamma_\ell(k) Y_{\ell,m_\ell}(\hat{\mathbf{k}}) a_{\mathbf{k}+\mathbf{q}/2,\uparrow} a_{\mathbf{k}-\mathbf{q}/2,\downarrow}$ and $\xi_\ell(\mathbf{k}) = \epsilon(\mathbf{k}) - \mu_\ell$. We first introduce the Nambu spinor $\psi^\dagger(p) = (a^\dagger_{p,\uparrow}, a_{-p,\downarrow})$, where $p = (\mathbf{k}, iw_j)$ denotes both momentum and Fermionic Matsubara frequency $w_j = (2j+1)\pi/\beta$, and use a Hubbard-Stratonovich transformation to decouple Fermionic and Bosonic degrees of freedom. Integration over the Fermionic part $[D(\psi^\dagger, \psi)]$ leads to the action

$$S_\ell^{\text{eff}} = \beta \sum_{q,m_\ell} \frac{|\Phi_{\ell,m_\ell}(q)|^2}{4\pi\mathcal{V}^{-1}\lambda_\ell} + \sum_{p,q} [\beta \xi_\ell(\mathbf{k}) \delta_{q,0} - \text{Tr} \ln(\mathbf{G}_\ell/\beta)^{-1}], \tag{5}$$

where $q = (\mathbf{q}, iv_j)$, with Bosonic Matsubara frequency $v_j = 2\pi j/\beta$. Here, $\mathbf{G}_\ell^{-1} = \Phi^*_\ell(q)\Gamma_\ell(p)\sigma_- + \Phi_\ell(-q)\Gamma_\ell(p)\sigma_+ + [iw_j\sigma_0 - \xi_\ell(\mathbf{k})\sigma_3]\delta_{q,0}$ is the inverse Nambu propagator, $\Phi_\ell(q) = \Sigma_{m_\ell} \Phi_{\ell,m_\ell}(q) Y_{\ell,m_\ell}(\hat{\mathbf{k}})$ is the Bosonic field, and $\sigma_\pm = (\sigma_1 \pm \sigma_2)/2$ and σ_i is the Pauli spin matrix. The Bosonic field $\Phi_{\ell,m_\ell}(q) = \Delta_{\ell,m_\ell}\delta_{q,0} + \Lambda_{\ell,m_\ell}(q)$ has τ-independent Δ_{ℓ,m_ℓ} and τ-dependent $\Lambda_{\ell,m_\ell}(q)$ parts.

Performing an expansion in S_ℓ^{eff} to quadratic order in $\Lambda_{\ell,m_\ell}(q)$ leads to

$$S_\ell^{\text{gauss}} = S_\ell^{\text{sp}} + \frac{\beta}{2} \sum_{q,m_\ell,m'_\ell} \tilde{\Lambda}^\dagger_{\ell,m_\ell}(q) \mathbf{F}^{-1}_{\ell,m_\ell,m'_\ell}(q) \tilde{\Lambda}_{\ell,m'_\ell}(q), \tag{6}$$

where the vector $\tilde{\Lambda}^\dagger_{\ell,m_\ell}(q)$ is such that $\tilde{\Lambda}^\dagger_{\ell,m_\ell}(q) = [\Lambda^\dagger_{\ell,m_\ell}(q), \Lambda_{\ell,m_\ell}(-q)]$, and $\mathbf{F}^{-1}_{\ell,m_\ell,m'_\ell}(q)$ are the matrix elements of the inverse fluctuation propagator matrix $\mathbf{F}_\ell^{-1}(q)$. Furthermore, S_ℓ^{sp} is the saddle-point action given by $S_\ell^{\text{sp}} = \beta \Sigma_{m_\ell} \frac{|\Delta_{\ell,m_\ell}|^2}{4\pi\mathcal{V}^{-1}\lambda_\ell} + \Sigma_p [\beta\xi_\ell(\mathbf{k}) - \text{Tr} \ln(\mathbf{G}_\ell^{\text{sp}}/\beta)^{-1}]$, and the saddle-point inverse Nambu propagator is $(\mathbf{G}_\ell^{\text{sp}})^{-1} = iw_j\sigma_0 - \xi_\ell(\mathbf{k})\sigma_3 + \Delta^*_\ell(\mathbf{k})\sigma_- + \Delta_\ell(\mathbf{k})\sigma_+$, with saddle-point order parameter $\Delta_\ell(\mathbf{k}) = \Gamma_\ell(k) \Sigma_{m_\ell} \Delta_{\ell,m_\ell} Y_{\ell,m_\ell}(\hat{\mathbf{k}})$. Notice that $\Delta_\ell(\mathbf{k})$ may involve several different m_ℓ for a given angular momentum channel ℓ.

The matrix elements of the inverse fluctuation matrix $\mathbf{F}_\ell^{-1}(q)$ are given by

$$(\mathbf{F}^{-1}_{\ell,m_\ell,m'_\ell})_{11} = -\frac{1}{\beta} \sum_p (\mathbf{G}^{\text{sp}}_\ell)_{11}\left(\frac{q}{2} + p\right)(\mathbf{G}^{\text{sp}}_\ell)_{11}\left(\frac{q}{2} - p\right) \times \Gamma^2_\ell(p) Y_{\ell,m_\ell}(\hat{\mathbf{k}}) Y^*_{\ell,m'_\ell}(\hat{\mathbf{k}}) + \frac{\delta_{m_\ell,m'_\ell}\mathcal{V}}{4\pi\lambda_\ell}, \tag{7}$$

$$(\mathbf{F}^{-1}_{\ell,m_\ell,m'_\ell})_{12} = \frac{1}{\beta} \sum_p (\mathbf{G}^{\text{sp}}_\ell)_{12}\left(\frac{q}{2} + p\right)(\mathbf{G}^{\text{sp}}_\ell)_{12}\left(\frac{q}{2} - p\right) \times \Gamma^2_\ell(p) Y_{\ell,m_\ell}(\hat{\mathbf{k}}) Y^*_{\ell,m'_\ell}(\hat{\mathbf{k}}). \tag{8}$$

Notice that while $(\mathbf{F}^{-1}_{\ell,m_\ell,m'_\ell})_{12}(q) = (\mathbf{F}^{-1}_{\ell,m_\ell,m'_\ell})_{21}(q)$ are even under the transformations $\mathbf{q} \to -\mathbf{q}$ and $iv_j \to -iv_j$; $(\mathbf{F}^{-1}_{\ell,m_\ell,m'_\ell})_{11}(q) = (\mathbf{F}^{-1}_{\ell,m_\ell,m'_\ell})_{22}(-q)$ are even only under $\mathbf{q} \to -\mathbf{q}$, having no defined parity in iv_j.

The Gaussian action Eq. (6) leads to the thermodynamic potential $\Omega_\ell^{\text{gauss}} = \Omega_\ell^{\text{sp}} + \Omega_\ell^{\text{fluct}}$, where

$$\Omega_\ell^{\text{sp}} = \sum_{m_\ell} \frac{|\Delta_{\ell,m_\ell}|^2}{4\pi\mathcal{V}^{-1}\lambda_\ell} + \sum_{\mathbf{k}} \left(\xi_\ell(\mathbf{k}) - E_\ell(\mathbf{k}) - \frac{2}{\beta} \ln\{1 + \exp[-\beta E_\ell(\mathbf{k})]\} \right), \tag{9}$$

$$\Omega_\ell^{\text{fluct}} = \frac{1}{\beta} \sum_q \ln \det[\mathbf{F}_\ell^{-1}(q)/(2\beta)] \tag{10}$$

are the saddle-point and fluctuation contributions, respectively. Here, $E_\ell(\mathbf{k}) = [\xi^2_\ell(\mathbf{k}) + |\Delta_\ell(\mathbf{k})|^2]^{1/2}$ is the quasiparticle energy spectrum. Having completed the presentation of the functional integral formalism, we discuss next the self-consistency equations for the order parameter and the chemical potential.

B. Self-consistency equations

The saddle-point condition $\delta S_\ell^{\text{sp}}/\delta\Delta^*_{\ell,m_\ell} = 0$ leads to the order-parameter equation

$$\frac{\Delta_{\ell,m_\ell}}{4\pi\lambda_\ell} = \frac{1}{\mathcal{V}} \sum_{\mathbf{k}} \frac{\Delta_\ell(\mathbf{k})\Gamma_\ell(k) Y^*_{\ell,m_\ell}(\hat{\mathbf{k}})}{2E_\ell(\mathbf{k})} \tanh \frac{\beta E_\ell(\mathbf{k})}{2}, \tag{11}$$

which can be expressed in terms of experimentally relevant parameters via the T-matrix approach [32].

The low-energy two-body scattering amplitude between a pair of fermions in the ℓth angular momentum channel is given by [38]

$$f_\ell(k) = -\frac{k^{2\ell}}{1/a_\ell - r_\ell k^2 + ik^{2\ell+1}}, \tag{12}$$

where $r_\ell < 0$ and a_ℓ are the effective range and scattering parameter, respectively. Here r_ℓ has dimensions of $L^{2\ell-1}$ and a_ℓ has dimensions of $L^{2\ell+1}$, where L is the size of the system. The energy of the two-body bound state is determined from the poles of $f_\ell(k \to i\kappa_\ell)$, and is given by $E_{\text{b},\ell} = -\kappa_\ell^2/(2M)$. Bound states occur when $a_0 > 0$ for $\ell = 0$, and $a_{\ell\neq 0} r_{\ell\neq 0} < 0$ for $\ell \neq 0$. Since $r_\ell < 0$, bound states occur only when $a_\ell > 0$ for all ℓ, in which case the binding energies are given by

$$E_{\text{b},0} = -\frac{1}{Ma_0^2}, \tag{13}$$

$$E_{\text{b},\ell\neq 0} = \frac{1}{Ma_\ell r_\ell}. \tag{14}$$

Notice that only a single parameter (a_0) is sufficient to describe the low-energy two-body problem for $\ell = 0$, while two parameters (a_ℓ, r_ℓ) are necessary to describe the same problem for $\ell \neq 0$. The point at which $1/(k_{\text{F}}^{2\ell+1} a_\ell) = 0$ corresponds to the threshold for the formation of a two-body bound state in vacuum. Beyond this threshold, a_0 for $\ell = 0$ and $|a_{\ell\neq 0} r_{\ell\neq 0}|$ for $\ell \neq 0$ are the size of the bound states.

For any ℓ, the two-body scattering amplitude is related to the T matrix via $f_\ell(k)=-M/(4\pi)T_\ell[k,k;2\epsilon(\mathbf{k})+i0^+]$, where the T matrix is given by

$$T(\mathbf{k},\mathbf{k}',E) = V(\mathbf{k},\mathbf{k}') + \frac{1}{\mathcal{V}}\sum_{\mathbf{k}''} \frac{V(\mathbf{k},\mathbf{k}'')T(\mathbf{k}'',\mathbf{k}',E)}{E-2\epsilon(\mathbf{k}'')+i0^+}.$$

Using the spherical harmonics expansion for both $V(\mathbf{k},\mathbf{k}')$ and $T(\mathbf{k},\mathbf{k}',E)$ leads to two coupled equations,

$$\frac{1}{\lambda_\ell} = -\frac{M}{4\pi k_0^{2\ell} a_\ell} + \frac{1}{\mathcal{V}}\sum_{\mathbf{k}} \frac{\Gamma_\ell^2(k)}{2\epsilon(\mathbf{k})}, \tag{15}$$

$$r_{\ell\neq 0} = -\frac{\pi k_0^{2\ell}}{M^2\mathcal{V}}\sum_{\mathbf{k}} \frac{\Gamma_\ell^2(k)}{\epsilon^2(\mathbf{k})} - \frac{\ell+1}{k_0^2 a_\ell}, \tag{16}$$

relating λ_ℓ and k_0 to a_ℓ and r_ℓ. Except for notational differences, notice that these relations are identical to previous results [32]. After performing momentum integrations we obtain

$$k_0^{2\ell+1} a_\ell = \frac{M k_0 \lambda_\ell \sqrt{\pi}}{M k_0 \lambda_\ell \tilde{\phi}_\ell - 4\pi\sqrt{\pi}}, \tag{17}$$

$$-\frac{1}{a_{\ell\neq 0} r_{\ell\neq 0}} = \frac{2k_0^2\sqrt{\pi}}{k_0^{2\ell+1} a_\ell \phi_\ell + 2(\ell+1)\sqrt{\pi}}, \tag{18}$$

where $\tilde{\phi}_\ell=\Gamma(\ell+1/2)/\Gamma(\ell+1)$ and $\phi_\ell=\Gamma(\ell-1/2)/\Gamma(\ell+1)$. Here $\Gamma(x)$ is the gamma function. Notice that $k_0^{2\ell+1}a_\ell$ diverges and changes sign when $Mk_0\lambda_\ell\tilde{\phi}_\ell=4\pi\sqrt{\pi}$, which corresponds to the critical coupling for Feshbach resonances (the unitarity limit).

In addition, the scattering parameter has a maximum value in the zero ($\lambda_\ell\to 0$) and a minimum value in the infinite ($\lambda_\ell\to\infty$) coupling limits given, respectively, by $k_0^{2\ell+1}a_{\ell\neq 0}^{\max}=-2(\ell+1)\sqrt{\pi}/\phi_\ell$ ($a_\ell<0$) and $k_0^{2\ell+1}a_\ell^{\min}=\sqrt{\pi}/\tilde{\phi}_\ell$ ($a_\ell>0$). The first condition (when $\lambda_\ell\to 0$) follows from Eq. (18) where $r_{\ell\neq 0}<0$ has to be satisfied for all possible $a_{\ell\neq 0}$. However, there is no condition on r_0 for $\ell=0$, and $k_0 a_0^{\max}=0$ in the BCS limit. The second condition (when $\lambda_\ell\to\infty$) follows from Eq. (17), which is valid for all possible ℓ. The minimum a_ℓ for a finite range interaction is associated with the Pauli principle, which prevents two identical fermions to occupy the same state. Thus while the scattering parameter cannot be arbitrarily small for a finite range potential, it may go to zero as $k_0\to\infty$. Furthermore, the binding energy is given by $E_{b,\ell\neq 0}=-2\sqrt{\pi}/(Mk_0^{2\ell-1}a_\ell\phi_\ell)$, when $k_0^{2\ell+1}a_\ell\phi_\ell \gg 2(\ell+1)\sqrt{\pi}$.

Thus the order-parameter equation in terms of the scattering parameter is rewritten as

$$\frac{M\mathcal{V}\Delta_{\ell,m_\ell}}{16\pi^2 k_0^{2\ell} a_\ell} = \sum_{\mathbf{k},m_\ell'}\left[\frac{1}{2\epsilon(\mathbf{k})} - \frac{\tanh[\beta E_\ell(\mathbf{k})/2]}{2E_\ell(\mathbf{k})}\right] \times \Delta_{\ell,m_\ell'}\Gamma_\ell^2(k) Y_{\ell,m_\ell}^*(\hat{\mathbf{k}}) Y_{\ell,m_\ell'}(\hat{\mathbf{k}}). \tag{19}$$

This equation is valid for both THS pseudospin singlet and SHS pseudospin triplet states. However, there is one important difference between pseudospin singlet and pseudospin triplet states. For pseudospin singlet states, the order parameter is a scalar function of $\mathbf{k}$, while it is a vector function for pseudospin triplet states discussed next.

In general, the triplet order parameter can be written in the standard form [39]

$$\mathbf{O}_\ell(\mathbf{k}) = \begin{pmatrix} -d_\ell^x(\mathbf{k}) + id_\ell^y(\mathbf{k}) & d_\ell^z(\mathbf{k}) \\ d_\ell^z(\mathbf{k}) & d_\ell^x(\mathbf{k}) + id_\ell^y(\mathbf{k}) \end{pmatrix}, \tag{20}$$

where the vector $d_\ell(\mathbf{k})=[d_\ell^x(\mathbf{k}),d_\ell^y(\mathbf{k}),d_\ell^z(\mathbf{k})]$ is an odd function of $\mathbf{k}$. Therefore all up-up, down-down, and up-down components may exist for a THS pseudospin triplet interaction. However, in the SHS pseudospin triplet case only the up-up or down-down component may exist leading to $\Delta_\ell(\mathbf{k})\propto(\mathbf{O}_\ell)_{s_1 s_1}(\mathbf{k})$. Thus for the up-up case $d_\ell^z(\mathbf{k})=0$ and $d_\ell^x(\mathbf{k})=-id_\ell^y(\mathbf{k})$, leading to $d_\ell(\mathbf{k})=d_\ell^x(\mathbf{k})(1,i,0)$, which breaks time-reversal symmetry, as expected from a fully spin polarized state. The corresponding down-down state has $d_\ell(\mathbf{k})=d_\ell^x(\mathbf{k})(1,-i,0)$. Furthermore, the simplified form of the SHS triplet order parameter allows a treatment similar to that of THS singlet states. However, it is important to mention that the THS triplet case can be investigated using our approach, but the treatment is more complicated.

The order-parameter equation has to be solved self-consistently with the number equation $N_\ell=-\partial\Omega_\ell/\partial\mu_\ell$ where Ω_ℓ is the full thermodynamic potential. In the approximations used, $N_\ell\approx N_\ell^{\text{gauss}}=N_\ell^{\text{sp}}+N_\ell^{\text{fluct}}$ has two contributions. The saddle-point contribution to the number equation is

$$N_\ell^{\text{sp}} = \sum_{\mathbf{k},s} n_\ell(\mathbf{k}), \tag{21}$$

where $n_\ell(\mathbf{k})$ is the momentum distribution given by

$$n_\ell(\mathbf{k}) = \frac{1}{2}\left[1 - \frac{\xi_\ell(\mathbf{k})}{E_\ell(\mathbf{k})}\tanh\frac{\beta E_\ell(\mathbf{k})}{2}\right]. \tag{22}$$

For the SHS triplet case, the summation over s is not present in N_ℓ^{sp}. The fluctuation contribution to the number equation is

$$N_\ell^{\text{fluct}} = -\frac{1}{\beta}\sum_q \frac{\partial[\det \mathbf{F}_\ell^{-1}(q)]/\partial\mu_\ell}{\det \mathbf{F}_\ell^{-1}(q)}, \tag{23}$$

where $\mathbf{F}_\ell^{-1}(q)$ is the inverse fluctuation matrix defined in Eqs. (7) and (8).

In the rest of the paper, we analyze analytically the superfluid properties at zero temperature (ground state) and near the critical temperatures for the THS singlet (only even ℓ) and the SHS triplet (only odd ℓ) cases. In addition, we analyze numerically the s-wave ($\ell=0$) channel of the THS singlet and the p-wave ($\ell=1$) channel of the SHS triplet cases, which are currently of intense theoretical and experimental interest in ultracold Fermi atoms.

IV. BCS TO BEC EVOLUTION AT $T=0$

At low temperatures, the saddle-point self-consistent (order parameter and number) equations are sufficient to describe ground-state properties in the weak-coupling BCS and

strong-coupling BEC limits [10]. However, fluctuation corrections to the number equation may be important in the intermediate regime [40].

Ground-state properties ($T=0$) are investigated by solving saddle-point self-consistency (order parameter and number) equations to obtain Δ_{ℓ,m_ℓ} and μ_ℓ, which are discussed next.

A. Order parameter and chemical potential

We discuss in this section Δ_{ℓ,m_ℓ} and μ_ℓ. In weak coupling, we first introduce a shell about the Fermi energy $|\xi_\ell(\mathbf{k})| \leqslant w_D$ such that $\epsilon_F \gg w_D \gg \Delta_\ell(\mathbf{k}_F)$, inside of which one may ignore the 3D density-of-states factor $(\sqrt{\epsilon/\epsilon_F})$ and outside of which one may ignore $\Delta_\ell(\mathbf{k})$. While in sufficiently strong coupling, we use $\xi_\ell(\mathbf{k}) \gg |\Delta_\ell(\mathbf{k})|$ to derive the analytic results discussed below. It is important to notice that, in strictly weak and strong coupling, the self-consistency equations (21) and (19) are decoupled, and play reversed roles. In weak (strong) coupling the order-parameter equation determines Δ_{ℓ,m_ℓ} (μ_ℓ) and the number equation determine μ_ℓ (Δ_{ℓ,m_ℓ}).

In weak coupling, the number equation Eq. (21) leads to

$$\mu_\ell = \epsilon_F \tag{24}$$

for any ℓ where $\epsilon_F = k_F^2/(2M)$ is the Fermi energy. In strong coupling, the order-parameter equation (19) leads to

$$\mu_0 = -\frac{1}{2Ma_0^2}, \tag{25}$$

$$\mu_{\ell\neq 0} = -\frac{\sqrt{\pi}}{Mk_0^{2\ell-1}a_\ell\phi_\ell}, \tag{26}$$

where $\phi_\ell = \Gamma(\ell-1/2)/\Gamma(\ell+1)$ and $\Gamma(x)$ is the Gamma function. This calculation requires that $a_0k_0 > 1$ for $\ell=0$ and that $k_0^{2\ell+1}a_\ell\phi_\ell > (\ell+1)\sqrt{\pi}$ for $\ell \neq 0$ for the order-parameter equation to have a solution with $\mu_\ell < 0$ in the strong-coupling limit. In the BEC limit $\mu_0 = -k_0^2/[2M(k_0a_0-1)^2]$ for $\ell=0$. Notice that $\mu_0 = -1/(2Ma_0^2)$ when $k_0a_0 \gg 1$ [or $|\mu_0| \ll \epsilon_0 = k_0^2/(2M)$], and thus we recover the contact potential ($k_0 \to \infty$) result. In the same spirit, to obtain the expressions in Eqs. (25) and (26), we assumed $|\mu_\ell| \ll \epsilon_0$. Notice that $\mu_\ell = E_{b,\ell}/2$ in this limit for any ℓ.

On the other hand, the solution of the order-parameter equation in the weak-coupling limit is

$$|\Delta_{0,0}| = 16\sqrt{\pi}\epsilon_F \exp\left[-2 + \frac{\pi}{2}\frac{k_F}{k_0} - \frac{\pi}{2k_F|a_0|}\right], \tag{27}$$

$$|\Delta_{\ell\neq 0,m_\ell}| \sim \left(\frac{k_0}{k_F}\right)^\ell \epsilon_F \exp\left[t_\ell\left(\frac{k_0}{k_F}\right)^{2\ell-1} - \frac{\pi}{2k_F^{2\ell+1}|a_\ell|}\right], \tag{28}$$

where $t_1 = \pi/4$ and $t_{\ell>1} = \pi 2^{\ell+1}(2\ell-3)!!/\ell!$. These expressions are valid only when the exponential terms are small. The solution of the number equation in the strong-coupling limit is

$$|\Delta_{0,0}| = 8\epsilon_F\left(\frac{\mu_0}{9\epsilon_F}\right)^{1/4}, \tag{29}$$

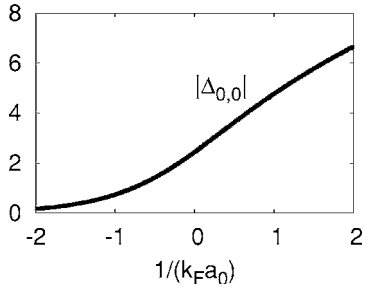

FIG. 1. Plot of reduced order parameter $\Delta_r = |\Delta_{0,0}|/\epsilon_F$ vs interaction strength $1/(k_Fa_0)$ for $k_0 \approx 200k_F$.

$$\sum_{m_\ell} |\Delta_{\ell\neq 0,m_\ell}|^2 = \frac{64\sqrt{\pi}}{3\phi_\ell}\epsilon_F(\epsilon_F\epsilon_0)^{1/2} \tag{30}$$

to order μ_ℓ/ϵ_0, where we assumed that $\xi_\ell(\mathbf{k}) \gg |\Delta_\ell(\mathbf{k})|$ for sufficiently strong couplings with $|\mu_\ell| \ll \epsilon_0$.

Next, we present numerical results for two particular states. First, we analyze the THS s-wave ($\ell=0$, $m_\ell=0$) case, where $\Delta_0(\mathbf{k}) = \Delta_{0,0}\Gamma_0(k)Y_{0,0}(\hat{\mathbf{k}})$ with $Y_{0,0}(\hat{\mathbf{k}}) = 1/\sqrt{4\pi}$. Second, we discuss the SHS p-wave ($\ell=1$, $m_\ell=0$) case, where $\Delta_1(\mathbf{k}) = \Delta_{1,0}\Gamma_1(k)Y_{1,0}(\hat{\mathbf{k}})$ with $Y_{1,0}(\hat{\mathbf{k}}) = \sqrt{3/(4\pi)}\cos(\theta_{\mathbf{k}})$. In all numerical calculations, we choose $k_0 \approx 200k_F$ to compare s-wave and p-wave cases.

In Figs. 1 and 2, we show $|\Delta_{0,0}|$ and μ_0 at $T=0$ for the s-wave case. Notice that the BCS to BEC evolution range in $1/(k_Fa_0)$ is of order 1. Furthermore, $|\Delta_{0,0}|$ grows continuously without saturation with increasing coupling, while μ_0 changes from ϵ_F to $E_{b,0}/2$ continuously and decreases as $-1/(2Ma_0^2)$ for strong couplings. Thus the evolution of $|\Delta_{0,0}|$ and μ_0 as a function of $1/(k_Fa_0)$ is smooth. For completeness, it is also possible to obtain analytical values of a_0 and $\Delta_{0,0}$ when the chemical potential vanishes. When $\mu_0=0$, we obtain for $|\Delta_{0,0}| = 8\epsilon_F[\pi^2\sqrt{\pi}/\Gamma^4(1/4)]^{1/3} \approx 3.73\epsilon_F$ at $1/(k_Fa_0) = (2\pi^3\sqrt{\pi}\epsilon_F/|\Delta_{0,0}|)^{1/2}/[2\Gamma^2(3/4)] \approx 0.554$, which also agrees with the numerical results. Here $\Gamma(x)$ is the gamma function.

In Figs. 3 and 4, we show $|\Delta_{1,0}|$ and μ_1 at $T=0$ for the p-wave case. Notice that the BCS to BEC evolution range in $1/(k_F^3a_1)$ is of order k_0/k_F. Furthermore, $|\Delta_{1,0}|$ grows with increasing coupling but saturates for large $1/(k_F^3a_1)$, while μ_1 changes from ϵ_F to $E_{b,1}/2$ continuously and decreases as $-1/(Mk_0a_1)$ for strong couplings. For completeness, we

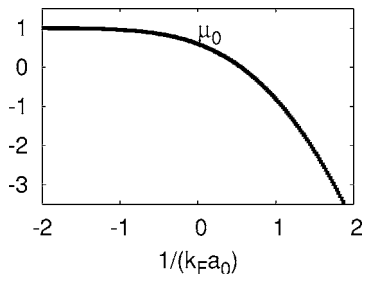

FIG. 2. Plot of reduced chemical potential $\mu_r = \mu_0/\epsilon_F$ (inset) vs interaction strength $1/(k_Fa_0)$ for $k_0 \approx 200k_F$.

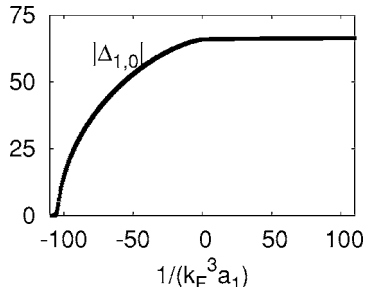

FIG. 3. Plots of reduced order parameter $\Delta_r=|\Delta_{1,0}|/\epsilon_F$ vs interaction strength $1/(k_F^3 a_1)$ for $k_0 \approx 200 k_F$.

present the limiting expressions $|\Delta_{1,0}|=24\frac{k_0}{k_F}\epsilon_F \exp\left[-\frac{8}{3}+\frac{\pi k_0}{4k_F}-\frac{\pi}{2k_F^3|a_1|}\right]$ and $|\Delta_{1,0}|=8\epsilon_F\left(\frac{\epsilon_0}{9\epsilon_F}\right)^{1/4}$, in the weak- and strong-coupling limits, respectively.

The evolution of $|\Delta_{1,0}|$ and μ_1 are qualitatively similar to recent $T=0$ results for THS fermion [32] and SHS fermion-boson [26] models. Due to the angular dependence of $\Delta_1(\mathbf{k})$, the quasiparticle excitation spectrum $E_1(\mathbf{k})$ is gapless for $\mu_1>0$, and fully gapped for $\mu_1<0$. Furthermore, both $\Delta_{1,0}$ and μ_1 are nonanalytic exactly when μ_1 crosses the bottom of the fermion energy band $\mu_1=0$ at $1/(k_F^3 a_1)\approx 0.48$. The nonanalyticity does not occur in the first derivative of $\Delta_{1,0}$ or μ_1 as it is the case in two dimensions [35], but occurs in the second and higher derivatives. Thus, in the p-wave case, the BCS to BEC evolution is not a crossover, but a quantum phase transition occurs, as can be seen in the quasiparticle excitation spectrum to be discussed next.

B. Quasiparticle excitations

The quasiparticle excitation spectrum $E_\ell(\mathbf{k})=[\xi_\ell^2(\mathbf{k})+|\Delta_\ell(\mathbf{k})|^2]^{1/2}$ is gapless at $\mathbf{k}$-space regions where the conditions $\Delta_\ell(\mathbf{k})=0$ and $\epsilon(\mathbf{k})=\mu_\ell$ are both satisfied. Notice that the second condition is only satisfied in the BCS side $\mu_\ell \geqslant 0$, and therefore the excitation spectrum is always gapped in the BEC side ($\mu_\ell<0$).

For $\ell=0$, the order parameter is isotropic in $\mathbf{k}$ space without zeros (nodes) since it does not have any angular dependence. Therefore the quasiparticle excitation spectrum is fully gapped in both BCS ($\mu_0>0$) and BEC ($\mu_0<0$) sides, since

$$\min\{E_0(\mathbf{k})\}=|\Delta_0(k_{\mu_0})| \quad (\mu_0>0), \tag{31}$$

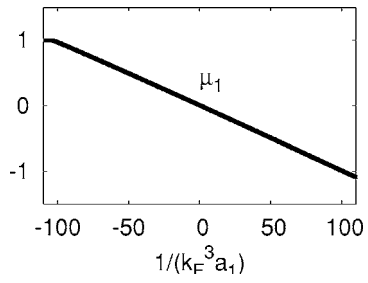

FIG. 4. Plots of reduced chemical potential $\mu_r=\mu_1/\epsilon_F$ (inset) vs interaction strength $1/(k_F^3 a_1)$ for $k_0 \approx 200 k_F$.

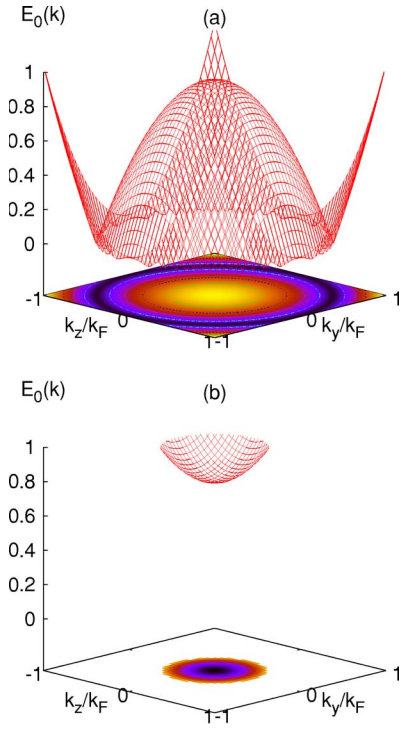

FIG. 5. (Color online) Plots of quasiparticle excitation spectrum $E_0(k_x=0,k_y,k_z)$ when (a) $\mu_0>0$ (BCS side) for $1/(k_F a_0)=-1$ and (b) $\mu_0<0$ (BEC side) for $1/(k_F a_0)=1$ vs momentum k_y/k_F and k_z/k_F.

$$\min\{E_0(\mathbf{k})\}=\sqrt{|\Delta_0(0)|^2+\mu_0^2} \quad (\mu_0<0). \tag{32}$$

Here, $k_{\mu_\ell}=\sqrt{2M\mu_\ell}$. This implies that the evolution of the quasiparticle excitation spectrum from weak-coupling BCS to strong-coupling BEC regime is smooth when $\mu_0=0$ for $\ell=0$ pairing.

In Fig. 5, we show $E_0(k_x=0,k_y,k_z)$ for an s-wave ($\ell=0$, $m_\ell=0$) superfluid when (a) $\mu_0>0$ (BCS side) for $1/(k_F a_0)=-1$ and (b) $\mu_0<0$ (BEC side) for $1/(k_F a_0)=1$. Notice that the quasiparticle excitation spectrum is gapped for both cases. However, the situation for $\ell\neq 0$ is very different as discussed next.

For $\ell\neq 0$, the order parameter is anisotropic in $\mathbf{k}$ space with zeros (nodes) since it has an angular dependence. Therefore while the quasiparticle excitation spectrum is gapless in the BCS ($\mu_{\ell\neq 0}>0$) side, it is fully gapped in the BEC ($\mu_{\ell\neq 0}<0$) side, since

$$\min\{E_{\ell\neq 0}(\mathbf{k})\}=0 \quad (\mu_\ell>0), \tag{33}$$

$$\min\{E_{\ell\neq 0}(\mathbf{k})\}=|\mu_\ell| \quad (\mu_\ell<0). \tag{34}$$

This implies that the evolution of quasiparticle excitation spectrum from weak-coupling BCS to strong-coupling BEC regime is not smooth for $\ell\neq 0$ pairing having a nonanalytic behavior when $\mu_{\ell\neq 0}=0$. This signals a quantum phase transition from a gapless to a fully gapped state exactly when $\mu_{\ell\neq 0}$ drops below the bottom of the energy band $\mu_{\ell\neq 0}=0$.

In Fig. 6, we show $E_1(k_x=0,k_y,k_z)$ for a p-wave ($\ell=1$, $m_\ell=0$) superfluid when (a) $\mu_1>0$ (BCS side) for $1/(k_F^3 a_1)$

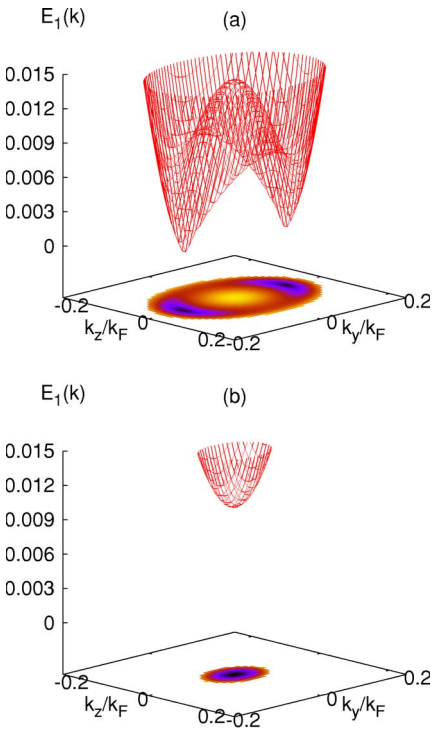

FIG. 6. (Color online) Plots of quasiparticle excitation spectrum $E_1(k_x=0,k_y,k_z)$ in (a) $\mu_1>0$ (BCS side) for $1/(k_F^3a_1)=-1$ and (b) $\mu_1<0$ (BEC side) for $1/(k_F^3a_1)=1$ vs momentum k_y/k_F and k_z/k_F.

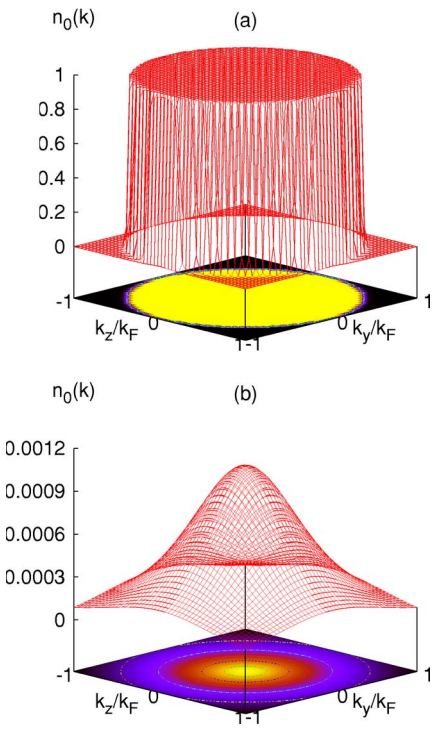

FIG. 7. (Color online) Contour plots of momentum distribution $n_0(k_x=0,k_y,k_z)$ when (a) $\mu_0>0$ (BCS side) for $1/(k_Fa_0)=-1$ and (b) $\mu_0<0$ (BEC side) for $1/(k_Fa_0)=1$ vs momentum k_y/k_F and k_z/k_F.

$=-1$ and (b) $\mu_1<0$ (BEC side) for $1/(k_F^3a_1)=1$. The quasiparticle excitation spectrum is gapless when $\Delta_1(\mathbf{k})\propto k_z/k_F=0$ and $k_x^2+k_y^2+k_z^2=2M\mu_1$ are both satisfied in certain regions of $\mathbf{k}$ space. For $k_x=0$, these conditions are met only when $k_z=0$ and $k_y=\pm\sqrt{2M\mu_1}$ for a given μ_1. Notice that these points come closer as the interaction (μ_1) increases (decreases), and when $\mu_1=0$ they become degenerate at $\mathbf{k}=\mathbf{0}$. For $\mu_1<0$, the second condition cannot be satisfied, and thus a gap opens in the excitation spectrum of quasiparticles as shown in Fig. 6(b).

The spectrum of quasiparticles plays an important role in the thermodynamic properties of the evolution from BCS to BEC regime at low temperatures. For $\ell=0$, thermodynamic quantities depend exponentially on T throughout the evolution. Thus a smooth crossover occurs at $\mu_0=0$. However, for $\ell\neq 0$, thermodynamic quantities depend exponentially on T only in the BEC side, while they have a power-law dependence on T in the BCS side. Thus a nonanalytic evolution occurs at $\mu_{\ell\neq 0}=0$. This can be seen best in the momentum distribution which is discussed next.

C. Momentum distribution

In this section, we analyze the momentum distribution $n_\ell(\mathbf{k})=[1-\xi_\ell(\mathbf{k})/E_\ell(\mathbf{k})]/2$ in the BCS ($\mu_\ell>0$) and BEC sides ($\mu_\ell<0$), which reflect the gapless to gapped phase transition for nonzero angular momentum superfluids.

In Fig. 7, we show $n_0(k_x=0,k_y,k_z)$ for an s-wave ($\ell=0,m_\ell=0$) superfluid when (a) $\mu_0>0$ (BCS side) for $1/(k_Fa_0)=-1$ and (b) $\mu_0<0$ (BEC side) for $1/(k_Fa_0)=1$. As the interaction increases the Fermi sea with locus $\xi_0(\mathbf{k})=0$ is suppressed, and pairs of atoms with opposite momenta become more tightly bound. As a result, $n_0(\mathbf{k})$ broadens in the BEC side since fermions with larger momentum participate in the formation of bound states. Notice that the evolution is a crossover without any qualitative change. Furthermore, $n_0(k_x,k_y=0,k_z)$ and $n_0(k_x,k_y,k_z=0)$ can be trivially obtained from $n_0(k_x=0,k_y,k_z)$, since $n_0(k_x,k_y,k_z)$ is symmetric in k_x, k_y, and k_z.

In Fig. 8, we show $n_1(k_x=0,k_y,k_z)$ for a p-wave ($\ell=1$, $m_\ell=0$) superfluid when (a) $\mu_1>0$ (BCS side) for $1/(k_F^3a_1)=-1$ and (b) $\mu_1<0$ (BEC side) for $1/(k_F^3a_1)=1$. Notice that $n_1(k_x=0,k_y,k_z)$ is largest in the BCS side when $k_z/k_F=0$, but it vanishes along $k_z/k_F=0$ for any k_y/k_F in the BEC side. As the interaction increases the Fermi sea with locus $\xi_1(\mathbf{k})=0$ is suppressed, and pairs of atoms with opposite momenta become more tightly bound. As a result, the large momentum distribution in the vicinity of $\mathbf{k}=\mathbf{0}$ splits into two peaks around finite $\mathbf{k}$ reflecting the p-wave symmetry of these tightly bound states. Furthermore, $n_1(k_x,k_y,k_z=0)=\{1-\mathrm{sgn}[\xi_1(\mathbf{k})]\}/2$ for any μ_1, and $n_1(k_x,k_y=0,k_z)$ is trivially obtained from $n_1(k_x=0,k_y,k_z)$, since $n_1(\mathbf{k})$ is symmetric in k_x,k_y. Here, sgn is the sign function.

Thus $n_1(\mathbf{k})$ for the p-wave case has a major rearrangement in $\mathbf{k}$ space with increasing interaction, in sharp contrast to the s-wave case. This qualitative difference between p-wave and s-wave symmetries around $\mathbf{k}=\mathbf{0}$ explicitly shows a direct measurable consequence of the gapless to gapped quantum phase transition when $\mu_1=0$, since $n_1(\mathbf{k})$ depends explicitly on $E_1(\mathbf{k})$. These quantum phase transitions are present in all

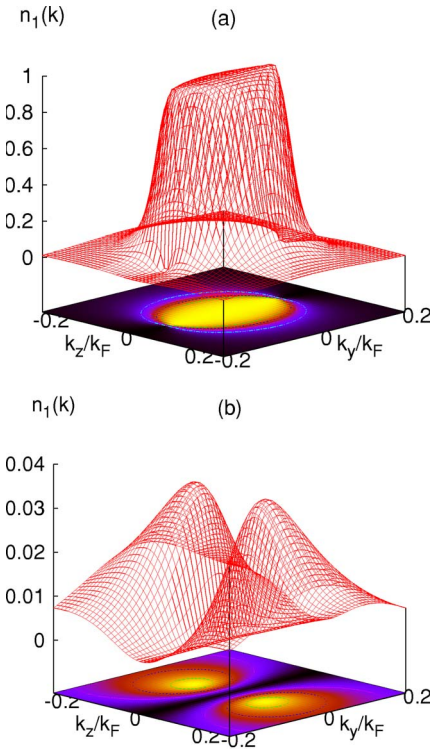

FIG. 8. (Color online) Contour plots of momentum distribution $n_1(k_x=0,k_y,k_z)$ in (a) $\mu_1>0$ (BCS side) for $1/(k_F^3a_1)=-1$ and (b) $\mu_1<0$ (BEC side) for $1/(k_F^3a_1)=1$ vs momentum k_y/k_F and k_z/k_F.

nonzero angular momentum states, and can be further characterized through the atomic compressibility as discussed in the next section.

D. Atomic compressibility

At finite temperatures, the isothermal atomic compressibility is defined by $\kappa_\ell^T(T)=-(\partial\mathcal{V}/\partial\mathcal{P})_{T,N_\ell}/\mathcal{V}$ where $\mathcal{V}$ is the volume and $\mathcal{P}$ is the pressure of the gas. This can be rewritten as

$$\kappa_\ell^T(T)=-\frac{1}{N_\ell^2}\left(\frac{\partial^2\Omega_\ell}{\partial\mu_\ell^2}\right)_{T,\mathcal{V}}=\frac{1}{N_\ell^2}\left(\frac{\partial N_\ell}{\partial\mu_\ell}\right)_{T,\mathcal{V}}, \tag{35}$$

where the partial derivative $\partial N_\ell/\partial\mu_\ell$ at $T\approx 0$ is given by $\frac{\partial N_\ell}{\partial\mu_\ell}\approx\frac{\partial N_\ell^{\rm sp}}{\partial\mu_\ell}=\Sigma_{\mathbf{k},s}\frac{|\Delta_\ell(\mathbf{k})|^2}{2E_\ell^3(\mathbf{k})}$.

The expression above leads to $\kappa_0^T(0)=2N(\epsilon_F)/N_0^2$ in weak-coupling BCS and $\kappa_0^T(0)=2N(\epsilon_F)\epsilon_F/(3|\mu_0|N_0^2)$ in strong-coupling BEC limit for $\ell=0$, where $N(\epsilon_F)=M\mathcal{V}k_F/(2\pi^2)$ is the density of states per spin at the Fermi energy. Notice that $\kappa_0^T(0)$ decreases as a_0^2 in strong coupling since $|\mu_0|=1/(2Ma_0^2)$. However, we only present the strong-coupling results for higher angular momentum states since they exhibit an interesting dependence on a_ℓ and k_0. In the case of THS pseudospin singlet, we obtain $\kappa_{\ell>1}^T(0)=4N(\epsilon_F)\epsilon_F\bar{\phi}_\ell/(\epsilon_0\phi_\ell N_\ell^2)$ for $\ell>1$, while in the case of SHS states we obtain $\kappa_1^T(0)=N(\epsilon_F)\epsilon_F/(\sqrt{\epsilon_0|\mu_1|}N_\ell^2)$ for $\ell=1$ and $\kappa_{\ell>1}^T(0)=2N(\epsilon_F)\epsilon_F\bar{\phi}_\ell/(\epsilon_0\phi_\ell N_\ell^2)$ for $\ell>1$. Here $\phi_\ell=\Gamma(\ell-1/2)/\Gamma(\ell+1)$ and $\bar{\phi}_\ell=\Gamma(\ell-3/2)/\Gamma(\ell+1)$, where $\Gamma(x)$ is the gamma function. Notice that $\kappa_1^T(0)$ decreases as $\sqrt{a_1}$ for $\ell=1$ since $|\mu_1|=1(Mk_0a_1)$ and $\kappa_{\ell>1}^T(0)$ is a constant for $\ell>1$ in strong coupling.

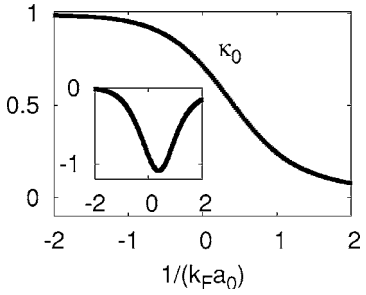

FIG. 9. Plot of reduced isothermal atomic compressibility $\kappa_r=\kappa_0^T(0)/\tilde{\kappa}_0$ vs interaction strength $1/(k_Fa_0)$ for $k_0\approx 200k_F$. The inset shows the numerical derivative of $d\kappa_r/d[(k_Fa_0)^{-1}]$ vs $1/(k_Fa_0)$. Here, $\tilde{\kappa}_0$ is the weak-coupling compressibility.

In Fig. 9, we show the evolution of $\kappa_0^T(0)$ for a s-wave $(\ell=0,m_\ell=0)$ superfluid from the BCS to the BEC regime. $\kappa_0^T(0)$ decreases continuously, and thus the evolution is a crossover (smooth) as can be seen in the inset where the numerical derivative of $\kappa_0^T(0)$ with respect to $1/(k_Fa_0)$ is shown $\{d\kappa_0^T(0)/d[(k_Fa_0)^{-1}]\}$. This decrease is associated with the increase of the gap of the excitation spectrum as a function of $1/(k_Fa_0)$. In this approximation, the gas is incompressible $[\kappa_0^T(0)\to 0]$ in the extreme BEC limit.

In Fig. 10, we show the evolution of $\kappa_1^T(0)$ for a p-wave $(\ell=1,\ m_\ell=0)$ superfluid from the BCS to the BEC regime. Notice that there is a change in qualitative behavior when $\mu_1=0$ at $1/(k_F^3a_1)\approx 0.48$ as can be seen in the inset where the numerical derivative of $\kappa_1^T(0)$ with respect to $1/(k_F^3a_1)$ is shown $\{d\kappa_1^T(0)/d[(k_F^3a_1)^{-1}]\}$. Thus the evolution from BCS to BEC is not a crossover, but a quantum phase transition occurs when $\mu_1=0$ [25,33–35].

The nonanalytic behavior occurring when $\mu_{\ell\neq 0}=0$ can be understood from higher derivatives of κ_ℓ with respect to μ_ℓ given by $\left[\frac{\partial\kappa_\ell^T(T)}{\partial\mu_\ell}\right]T,\mathcal{V}=-2N_\ell[\kappa_\ell^T(T)]2+\frac{1}{N_\ell^2}\left(\frac{\partial^2N_\ell}{\partial\mu_\ell^2}\right)_{T,\mathcal{V}}$. For instance, the second derivative $\partial^2N_\ell^{\rm sp}/\partial\mu_\ell^2=3\Sigma_{\mathbf{k},s}|\Delta_\ell(\mathbf{k})|^2\xi_\ell(\mathbf{k})/[2E_\ell^5(\mathbf{k})]$ tends to zero in the weak- $(\mu_\ell\approx\epsilon_F>0)$ and strong- $(\mu_\ell\approx E_{b,\ell}/2<0)$ coupling limits. On the other hand, when $\mu_\ell=0$, $\partial^2N_\ell^{\rm sp}/\partial\mu_\ell^2$ is finite only for

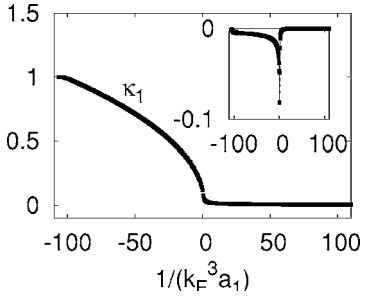

FIG. 10. Plot of reduced isothermal atomic compressibility $\kappa_r=\kappa_1^T(0)/\tilde{\kappa}_1$ vs interaction strength $1/(k_F^3a_1)$ for $k_0\approx 200k_F$. The inset shows the numerical derivative of $d\kappa_r/d[(k_F^3a_1)^{-1}]$ vs $1/(k_F^3a_1)$. Here $\tilde{\kappa}_1$ is the weak-coupling compressibility.

$\ell=0$, and it diverges for $\ell\neq 0$. This divergence is logarithmic for $\ell=1$, and of higher order for $\ell>1$. Thus we conclude again that higher derivatives of $N_\ell^{\rm sp}$ are nonanalytic when $\mu_{\ell\neq 0}=0$, and that a quantum phase transition occurs for $\ell\neq 0$.

Theoretically, the calculation of the isothermal atomic compressibility $\kappa_\ell^T(T)$ is easier than the isentropic atomic compressibility $\kappa_\ell^S(T)$. However, performing measurements of $\kappa_\ell^S(T)$ may be simpler in cold Fermi gases, since the gas expansion upon release from the trap is expected to be nearly isentropic. Fortunately, $\kappa_\ell^S(T)$ is related to $\kappa_\ell^T(T)$ via the thermodynamic relation $\kappa_\ell^S(T)=\frac{C_\ell^{\mathcal{V}}(T)}{C_\ell^{\mathcal{P}}(T)}\kappa_\ell^T(T)$, where $\kappa_\ell^T(T)>\kappa_\ell^S(T)$ since specific heat capacities $C_\ell^{\mathcal{P}}(T)>C_\ell^{\mathcal{V}}(T)$. Furthermore, at low temperatures $(T\approx 0)$ the ratio $C_\ell^{\mathcal{P}}(T)/C_\ell^{\mathcal{V}}(T)\approx$const, and therefore $\kappa_\ell^S(T\approx 0)\propto\kappa_\ell^T(T\approx 0)$. Thus we expect qualitatively similar behavior in both the isentropic and isothermal compressibilities at low temperatures $(T\approx 0)$.

The measurement of the atomic compressibility could also be performed via an analysis of particle density fluctuations [41,42]. As it is well known from thermodynamics [43], $\kappa_\ell^T(T)$ is connected to density fluctuations via the relation $\langle n_\ell^2\rangle-\langle n_\ell\rangle^2=T\langle n_\ell\rangle^2\kappa_\ell^T(T)$, where $\langle n_\ell\rangle$ is the average density of atoms. From the measurement of density fluctuations $\kappa_\ell^T(T)$ can be extracted at any temperature T.

It is important to emphasize that in this quantum phase transition at $\mu_{\ell\neq 0}=0$, the symmetry of the order parameter does not change as is typical in the Landau classification of phase transitions. However, a clear thermodynamic signature occurs in derivatives of the compressibility suggesting that the phase transition is higher than second order according to Ehrenfest's classification. Next, we discuss the phase diagram at zero temperature.

E. Phase diagram

To have a full picture of the evolution from the BCS to the BEC limit at $T=0$, it is important to analyze thermodynamic quantities at low temperatures. In particular, it is important to determine the quantum critical region (QCR) where a qualitative change occurs in quantities such as the specific heat, compressibility, and spin susceptibility. Here, we do not discuss in detail the QCR, but we analyze the contributions from quasiparticle excitations to thermodynamic properties. However, the discussion can be extended to include collective excitations [28] (see Sec. V).

Next, we point out a major difference between $\ell=0$ and $\ell\neq 0$ states in connection with the spectrum of the quasiparticle excitations (see Sec. IV B) and their contribution to low-temperature thermodynamics.

For $\ell=0$, quasiparticle excitations are gapped for all couplings, and therefore thermodynamic quantities such as atomic compressibility, specific heat, and spin susceptibility have an exponential dependence on the temperature and the minimum energy of quasiparticle excitations $\sim\exp[-\min\{E_0(\mathbf{k})\}/T]$. Using Eqs. (31) and (32) leads to $\sim\exp[-|\Delta_0(k_{\mu_0})|/T]$ in the BCS side $(\mu_0>0)$ and $\sim\exp[-\sqrt{|\Delta_0(0)|^2+\mu_0^2}/T]$ in the BEC side $(\mu_0<0)$ as shown in Fig. 11, where $k_{\mu_\ell}=\sqrt{2M\mu_\ell}$. Notice that there is no qualitative change across $\mu_0=0$ at small but finite temperatures. This indicates the absence of a QCR and confirms there is only a crossover for s-wave $(\ell=0)$ superfluids at $T=0$.

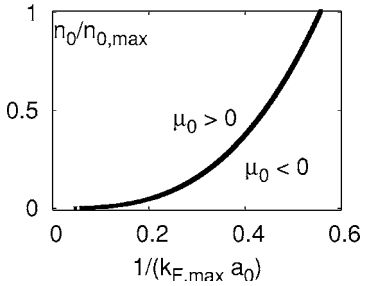

FIG. 11. The phase diagram of s-wave superfluids as a function of $1/(k_F a_0)$.

For $\ell\neq 0$, quasiparticle excitations are gapless in the BCS side and are only gapped in the BEC side, and therefore while thermodynamic quantities such as atomic compressibility, specific heat, and spin susceptibility have power-law dependences on the temperature $\sim T^{\beta_{\ell\neq 0}}$ in the BCS side, they have exponential dependences on the temperature and the minimum energy of quasiparticle excitations $\sim\exp[-\min\{E_{\ell\neq 0}(\mathbf{k})\}/T]$ in the BEC side. Here, $\beta_{\ell\neq 0}$ is a real number which depends on particular ℓ state. For $\ell=1$, using Eqs. (33) and (34) leads to $\sim T^{\beta_1}$ in the BCS side $(\mu_1>0)$ and $\sim\exp(-|\mu_1|/T)$ in the BEC side $(\mu_1<0)$ as shown in Fig. 12. Notice the change in qualitative behavior across $\mu_1=0$ (as well as other $\ell\neq 0$ states) at small but finite temperatures. This change occurs within the QCR and signals the existence of a quantum phase transition $(T=0)$ for $\ell\neq 0$ superfluids.

V. GAUSSIAN FLUCTUATIONS

Next, we discuss the fluctuation effects at zero temperature. The pole structure of $\mathbf{F}_\ell(\mathbf{q},iv_j)$ determines the two-particle excitation spectrum of the superconducting state with $iv_j\to w+i0^+$, and has to be taken into account to derive $\Omega_\ell^{\rm fluct}$. The matrix elements of $\mathbf{F}_\ell(\mathbf{q},iv_j)$ are $\mathbf{F}_{\ell,m_\ell,m_\ell'}(\mathbf{q},iv_j)$ for a given ℓ. We focus here only on the zero-temperature limit and analyze the collective phase modes. In this limit, we separate the diagonal matrix elements of $\mathbf{F}^{-1}_{\ell,m_\ell,m_\ell'}(q)$ into even and odd contributions with respect to iv_j,

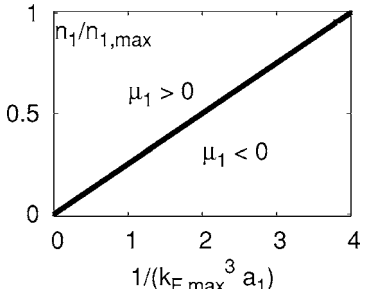

FIG. 12. The phase diagram of p-wave superfluids as a function of $1/(k_F^3 a_1)$.

$$(\mathbf{F}^{-1}_{\ell,m_\ell,m'_\ell})^E_{11} = \sum_{\mathbf{k}} \frac{(\xi_+\xi_- + E_+E_-)(E_+ + E_-)}{2E_+E_-[(iv_j)^2 - (E_+ + E_-)^2]} \Gamma^2_\ell(k) Y_{\ell,m_\ell}(\hat{\mathbf{k}}) \times Y^*_{\ell,m'_\ell}(\hat{\mathbf{k}}) - \frac{\delta_{m_\ell,m'_\ell}\mathcal{V}}{4\pi\lambda_\ell}, \tag{36}$$

$$(\mathbf{F}^{-1}_{\ell,m_\ell,m'_\ell})^O_{11} = -\sum_{\mathbf{k}} \frac{(\xi_+E_- + \xi_-E_+)(iv_j)}{2E_+E_-[(iv_j)^2 - (E_+ + E_-)^2]} \Gamma^2_\ell(k) \times Y_{\ell,m_\ell}(\hat{\mathbf{k}}) Y^*_{\ell,m'_\ell}(\hat{\mathbf{k}}). \tag{37}$$

The off-diagonal term is even in iv_j, and it reduces to

$$(\mathbf{F}^{-1}_{\ell,m_\ell,m'_\ell})_{12} = -\sum_{\mathbf{k}} \frac{\Delta_+\Delta_-(E_+ + E_-)}{2E_+E_-[(iv_j)^2 - (E_+ + E_-)^2]} \times \Gamma^2_\ell(k) Y_{\ell,m_\ell}(\hat{\mathbf{k}}) Y^*_{\ell,m'_\ell}(\hat{\mathbf{k}}). \tag{38}$$

Here the labels $\pm$ denote that the corresponding variables are functions of $\mathbf{k} \pm \mathbf{q}/2$.

In order to obtain the collective mode spectrum, we express $\Lambda_{\ell,m_\ell}(q) = \tau_{\ell,m_\ell}(q) e^{i\vartheta_{\ell,m_\ell}(q)} = [\rho_{\ell,m_\ell}(q) + i\theta_{\ell,m_\ell}(q)]/\sqrt{2}$ where $\tau_{\ell,m_\ell}(q)$, $\vartheta_{\ell,m_\ell}(q)$, $\rho_{\ell,m_\ell}(q)$, and $\theta_{\ell,m_\ell}(q)$ are all real. Notice that the new fields $\rho_{\ell,m_\ell}(q) = \tau_{\ell,m_\ell}(q)\cos[\vartheta_{\ell,m_\ell}(q)]$ and $\theta_{\ell,m_\ell}(q) = \tau_{\ell,m_\ell}(q)\sin[\vartheta_{\ell,m_\ell}(q)]$ can be regarded essentially as the amplitude and phase fields, respectively, when $\vartheta_{\ell,m_\ell}(q)$ is small. This change of basis can be described by the following unitary transformation:

$$\Lambda_{\ell,m_\ell}(q) = \frac{1}{\sqrt{2}} \begin{pmatrix} 1 & i \\ 1 & -i \end{pmatrix} \begin{bmatrix} \rho_{\ell,m_\ell}(q) \\ \theta_{\ell,m_\ell}(q) \end{bmatrix}.$$

From now on, we take Δ_{ℓ,m_ℓ} as real without loss of generality. The diagonal elements of the fluctuation matrix in the rotated basis are $(\tilde{\mathbf{F}}^{-1}_{\ell,m_\ell,m'_\ell})_{11} = (\mathbf{F}^{-1}_{\ell,m_\ell,m'_\ell})^E_{11} + (\mathbf{F}^{-1}_{\ell,m_\ell,m'_\ell})_{12}$, and $(\tilde{\mathbf{F}}^{-1}_{\ell,m_\ell,m'_\ell})_{22} = (\mathbf{F}^{-1}_{\ell,m_\ell,m'_\ell})^E_{11} - (\mathbf{F}^{-1}_{\ell,m_\ell,m'_\ell})_{12}$; and the off-diagonal elements are $(\tilde{\mathbf{F}}^{-1}_{\ell,m_\ell,m'_\ell})_{12} = (\tilde{\mathbf{F}}^{-1}_{\ell,m_\ell,m'_\ell})^*_{21} = i(\mathbf{F}^{-1}_{\ell,m_\ell,m'_\ell})^O_{11}$ with the q dependence being implicit.

A. Collective (Goldstone) modes

The collective modes are determined by the poles of the propagator matrix $\mathbf{F}_\ell(q)$ for the pair fluctuation fields $\Lambda_{\ell,m_\ell}(q)$, which describe the Gaussian deviations about the saddle-point order parameter. The poles of $\mathbf{F}_\ell(q)$ are determined by the condition $\det \mathbf{F}^{-1}_\ell(q) = 0$, which leads to $2(2\ell+1)$ collective (amplitude and phase) modes, when the usual analytic continuation $iv_j \to w + i0^+$ is performed. Among them, there are $2\ell+1$ amplitude modes which we do not discuss here.

The easiest way to get the phase collective modes is to integrate out the amplitude fields to obtain a phase-only effective action. Notice that for $\ell \neq 0$ channels at any temperature, and for $\ell = 0$ channel at finite temperature, a well defined low-frequency expansion is not possible for $\mu_\ell > 0$ due to Landau damping which causes the collective modes to decay into the two quasiparticle continuum. A well defined expansion [collective mode dispersion w] must satisfy the following condition: $w \ll \min\{E_+ + E_-\}$. Thus a zero-temperature expansion is always possible when Landau damping is subdominant (underdamped regime). To obtain the long-wavelength dispersions for the collective modes at $T=0$, we expand the matrix elements of $\tilde{\mathbf{F}}^{-1}_{\ell,m_\ell,m_\ell}$ to second order in $|\mathbf{q}|$ and w to get

$$(\tilde{\mathbf{F}}^{-1}_{\ell,m_\ell,m'_\ell})_{11} = A_{\ell,m_\ell,m'_\ell} + \sum_{i,j} C^{i,j}_{\ell,m_\ell,m'_\ell} q_i q_j - D_{\ell,m_\ell,m'_\ell} w^2, \tag{39}$$

$$(\tilde{\mathbf{F}}^{-1}_{\ell,m_\ell,m'_\ell})_{22} = P_{\ell,m_\ell,m'_\ell} + \sum_{i,j} Q^{i,j}_{\ell,m_\ell,m'_\ell} q_i q_j - R_{\ell,m_\ell,m'_\ell} w^2, \tag{40}$$

$$(\tilde{\mathbf{F}}^{-1}_{\ell,m_\ell,m'_\ell})_{12} = iB_{\ell,m_\ell,m'_\ell} w. \tag{41}$$

The expressions for the expansion coefficients are given in Appendix A.

For $\ell = 0$, the coefficients $C^{i,j}_{0,0,0} = C_{0,0,0}\delta_{i,j}$ and $Q^{i,j}_{0,0,0} = Q_{0,0,0}\delta_{i,j}$ are diagonal and isotropic in (i,j), and $P_{0,0,0} = 0$ vanishes. Here, $\delta_{i,j}$ is the Kronecker delta. Thus the collective mode is the isotropic Goldstone mode with dispersion

$$W_{0,0}(\mathbf{q}) = \mathcal{C}_{0,0}|\mathbf{q}|, \tag{42}$$

$$\mathcal{C}_{0,0} = \left(\frac{A_{0,0,0}Q_{0,0,0}}{A_{0,0,0}R_{0,0,0} + B^2_{0,0,0}} \right)^{1/2}, \tag{43}$$

where $\mathcal{C}_{0,0}$ is the speed of sound. Notice that the quasiparticle excitations are always fully gapped from weak to strong coupling, and thus the Goldstone mode is not damped at $T=0$ for all couplings.

For $\ell \neq 0$, the dispersion for collective modes is not easy to extract in general, and therefore we consider the case when only one of the spherical harmonics $Y_{\ell,m_\ell}(\hat{\mathbf{k}})$ is dominant and characterizes the order parameter. In this case, $P_{\ell,m_\ell,m_\ell} = 0$ due to the order-parameter equation, and the collective mode is the anisotropic Goldstone mode with dispersion

$$W_{\ell\neq 0,m_\ell}(\mathbf{q}) = \left[\sum_{i,j} (\mathcal{C}^{i,j}_{\ell,m_\ell})^2 q_i q_j \right]^{1/2}, \tag{44}$$

$$\mathcal{C}^{i,j}_{\ell\neq 0,m_\ell} = \left(\frac{A_{\ell,m_\ell,m_\ell} Q^{i,j}_{\ell,m_\ell,m_\ell}}{A_{\ell,m_\ell,m_\ell} R_{\ell,m_\ell,m_\ell} + B^2_{\ell,m_\ell,m_\ell}} \right)^{1/2}. \tag{45}$$

Notice that the speed of sound has a tensor structure and is anisotropic. Furthermore, the quasiparticle excitations are gapless when $\mu_{\ell\neq 0} > 0$, and thus the Goldstone mode is damped even at $T=0$. However, Landau damping is subdominant and the real part of the pole dominates for small momenta. In addition, quasiparticle excitations are fully gapped when $\mu_{\ell\neq 0} < 0$, and thus the Goldstone mode is not damped. Therefore the pole contribution to $\Omega^{\text{fluct}}_{\ell\neq 0}$ comes from the Goldstone mode for all couplings. In addition, there is

also a branch cut representing the continuum of two particle scattering states, but the contribution from the Goldstone mode dominates at sufficiently low temperatures.

It is also illustrative to analyze the eigenvectors of $\tilde{\mathbf{F}}_\ell^{-1}(q)$ in the amplitude-phase representation corresponding to small $W_{\ell,m_\ell}(\mathbf{q})$ mode

$$\begin{bmatrix} \rho_{\ell,m_\ell}(q) \\ \theta_{\ell,m_\ell}(q) \end{bmatrix} = \begin{bmatrix} -i\dfrac{B_{\ell,m_\ell,m_\ell}}{A_{\ell,m_\ell,m_\ell}} W_{\ell,m_\ell}(\mathbf{q}) \\ 1 \end{bmatrix}.$$

Notice that, when $B_{\ell,m_\ell,m_\ell} \to 0$ the amplitude and phase modes are not mixed.

Next, we discuss the dispersion of collective modes in the weak- and strong-coupling limits, where the expansion coefficients are analytically tractable for a fixed (ℓ, m_ℓ) state.

B. Weak-coupling (BCS) regime

The s-wave $(\ell=0, m_\ell=0)$ weak-coupling limit is characterized by the criteria $\mu_0 > 0$ and $\mu_0 \approx \epsilon_F \gg |\Delta_{0,0}|$. The expansion of the matrix elements to order $|\mathbf{q}|^2$ and w^2 is performed under the condition $[w, |\mathbf{q}|^2/(2M)] \ll |\Delta_{0,0}|$. Analytic calculations are particularly simple in this case since all integrals for the coefficients needed to calculate the collective-mode dispersions are peaked near the Fermi surface. We first introduce a shell about the Fermi energy $|\xi_0(\mathbf{k})| \leqslant w_D$ such that $\epsilon_F \gg w_D \gg \Delta_0(\mathbf{k}_F)$, inside of which one may ignore the 3D density-of-states factor $\sqrt{\epsilon/\epsilon_F}$ and outside of which one may ignore $\Delta_0(\mathbf{k})$. In addition, we make use of the nearly perfect particle-hole symmetry, which forces integrals to vanish when their integrands are odd under the transformation $\xi_0(\mathbf{k}) \to -\xi_0(\mathbf{k})$. For instance, the coefficient that couple phase and amplitude modes vanish $(B_{0,0,0}=0)$ in this limit. Thus there is no mixing between phase and amplitude fields in weak coupling, as can be seen by inspection of the fluctuation matrix $\tilde{\mathbf{F}}_0(q)$.

For $\ell=0$, the zeroth-order coefficient is

$$A_{0,0,0} = \frac{N(\epsilon_F)}{4\pi}, \tag{46}$$

and the second-order coefficients are

$$C^{i,j}_{0,0,0} = \frac{Q^{i,j}_{0,0,0}}{3} = \frac{N(\epsilon_F) v_F^2}{36|\Delta_{0,0}|^2}\delta_{i,j}, \tag{47}$$

$$D_{0,0,0} = \frac{R_{0,0,0}}{3} = \frac{N(\epsilon_F)}{12|\Delta_{0,0}|^2}. \tag{48}$$

Here, $v_F = k_F/M$ is the Fermi velocity and $N(\epsilon_F) = M\mathcal{V}k_F/(2\pi^2)$ is the density of states per spin at the Fermi energy.

In weak coupling, since $B^2_{\ell,m_\ell,m_\ell} \ll A_{\ell,m_\ell,m_\ell} R_{\ell,m_\ell,m_\ell}$, the sound velocity is simplified to $C^{i,j}_{\ell,m_\ell} \approx [Q^{i,j}_{\ell,m_\ell,m_\ell}/A_{\ell,m_\ell,m_\ell}]$ for any ℓ. Using the coefficients above in Eq. (43), for $\ell=0$, we obtain

$$\mathcal{C}_{0,0} = \frac{v_F}{\sqrt{3}} \tag{49}$$

which is the well-known Anderson-Bogoliubov relation. For $\ell \neq 0$, the expansion coefficients require more detailed and lengthy analysis, and therefore we do not discuss them here. On the other hand, the expansion coefficients can be calculated for any ℓ in the strong-coupling BEC regime, which is discussed next.

C. Strong-coupling (BEC) regime

The strong-coupling limit is characterized by the criteria $\mu_\ell < 0$, $|\mu_\ell| \ll \epsilon_0 = k_0^2/(2M)$, and $|\xi_\ell(\mathbf{k})| \gg |\Delta_\ell(\mathbf{k})|$. The expansion of the matrix elements to order $|\mathbf{q}|^2$ and w^2 is performed under the condition $[w, |\mathbf{q}|^2/(2M)] \ll |\mu_\ell|$. The situation encountered here is very different from the weak-coupling limit, because one can no longer invoke particle-hole symmetry to simplify the calculation of many of the coefficients appearing in the fluctuation matrix $\tilde{\mathbf{F}}_\ell(q)$. In particular, the coefficient $B_{\ell,m_\ell,m_\ell} \neq 0$ indicates that the amplitude and phase fields are mixed. Furthermore, $P_{\ell,m_\ell,m_\ell}=0$, since this coefficient reduces to the order-parameter equation in this limit.

For $\ell=0$, the zeroth-order coefficient is

$$A_{0,0,0} = \frac{\kappa|\Delta_{0,0}|^2}{8\pi|\mu_0|}, \tag{50}$$

the first-order coefficient is

$$B_{0,0,0} = \kappa, \tag{51}$$

and the second-order coefficients are

$$C^{i,j}_{0,0,0} = Q^{i,j}_{0,0,0} = \frac{\kappa}{4M}\delta_{i,j}, \tag{52}$$

$$D_{0,0,0} = R_{0,0,0} = \frac{\kappa}{8|\mu_0|}, \tag{53}$$

where $\kappa = N(\epsilon_F)/(32\sqrt{|\mu_0|\epsilon_F})$.

Using the expressions above in Eq. (43), we obtain the sound velocity

$$\mathcal{C}_{0,0} = \left(\frac{|\Delta_{0,0}|^2}{32M|\mu_0|\pi}\right)^{1/2} = v_F\sqrt{\frac{k_F a_0}{3\pi}}. \tag{54}$$

Notice that the sound velocity is very small and its smallness is controlled by the scattering length a_0. Furthermore, in the theory of weakly interacting dilute Bose gas, the sound velocity is given by $\mathcal{C}_{B,0} = 4\pi a_{B,0} n_{B,0}/M^2_{B,0}$. Making the identification that the density of pairs is $n_{B,0}=n_0/2$, the mass of the pairs is $M_{B,0}=2M$, and that the Bose scattering length is $a_{B,0}=2a_0$, it follows that Eq. (54) is identical to the Bogoliubov result $\mathcal{C}_{B,0}$. Therefore our result for the Fermionic system represents in fact a weakly interacting Bose gas in the strong-coupling limit. A better estimate for $a_{B,0} \approx 0.6a_0$ can be found in the literature [44–47]. This is also the case when we construct the TDGL equation in Sec. VII B.

For $\ell \neq 0$, the zeroth-order coefficient is

$$A_{\ell\neq 0,m_\ell,m_\ell} = \frac{15\hat{\phi}_\ell \tilde{\kappa}}{2\epsilon_0\sqrt{\pi}}|\Delta_{\ell,m_\ell}|^2 \gamma_{\ell,\{m_\ell\}}, \tag{55}$$

the first-order coefficient is

$$B_{\ell\neq 0,m_\ell,m'_\ell} = \frac{\phi_\ell \tilde{\kappa}}{\sqrt{\pi}}\delta_{m_\ell,m'_\ell}, \tag{56}$$

and the second-order coefficients are

$$C^{i,i}_{\ell\neq 0,m_\ell,m'_\ell} = Q^{i,i}_{\ell\neq 0,m_\ell,m'_\ell} = \frac{\phi_\ell \tilde{\kappa}}{4M\sqrt{\pi}}\delta_{m_\ell,m'_\ell}, \tag{57}$$

$$D_{1,m_\ell,m'_\ell} = R_{1,m_\ell,m'_\ell} = \frac{3\tilde{\kappa}}{8\sqrt{\epsilon_0|\mu_1|}}\delta_{m_\ell,m'_\ell}, \tag{58}$$

$$D_{\ell>1,m_\ell,m'_\ell} = R_{\ell>1,m_\ell,m'_\ell} = \frac{3\bar{\phi}_\ell \tilde{\kappa}}{4\sqrt{\pi\epsilon_0}}\delta_{m_\ell,m'_\ell}, \tag{59}$$

where $\tilde{\kappa}=N(\epsilon_F)/(32\sqrt{\epsilon_0\epsilon_F})$, $\phi_\ell=\Gamma(\ell-1/2)/\Gamma(\ell+1)$, $\bar{\phi}_\ell=\Gamma(\ell-3/2)/\Gamma(\ell+1)$, and $\hat{\phi}_\ell=\Gamma(2\ell-3/2)/\Gamma(2\ell+2)$. Here $\Gamma(x)$ is the gamma function, and γ_{ℓ,m_ℓ} is an angular averaged quantity defined in AppendixB

In strong coupling, since $B^2_{\ell,m_\ell,m_\ell} \gg A_{\ell,m_\ell,m_\ell}R_{\ell,m_\ell,m_\ell}$, the sound velocity is simplified to $C^{i,j}_{\ell,m_\ell} \approx [A_{\ell,m_\ell,m_\ell}Q^{i,j}_{\ell,m_\ell,m_\ell}/B^2_{\ell,m_\ell,m_\ell}]^{1/2}$ for any ℓ. Using the expressions above in Eq. (45), for $\ell \neq 0$, we obtain

$$\mathcal{C}^{i,i}_{\ell\neq 0,m_\ell} = \left(\frac{15\gamma_{\ell,\{m_\ell\}}|\Delta_{\ell,m_\ell}|^2\hat{\phi}_\ell}{8M\phi_\ell\epsilon_0}\right)^{1/2} \tag{60}$$

$$= v_F\left(\frac{20\gamma_{\ell,\{m_\ell\}}\sqrt{\pi}\hat{\phi}_\ell}{\phi^2_\ell}\frac{k_F}{k_0}\right)^{1/2}. \tag{61}$$

Therefore the sound velocity is also very small and its smallness is controlled by the interaction range k_0 through the diluteness condition, i.e., $(k_0/k_F)^3 \gg 1$, for $\ell \neq 0$. Notice that the sound velocity is independent of the scattering parameter for $\ell \neq 0$.

Now, we turn our attention to a numerical analysis of the phase collective modes during the evolution from weak-coupling BCS to strong-coupling BEC limits.

D. Evolution from BCS to BEC regime

We focus only on s-wave ($\ell=0, m_\ell=0$) and p-wave ($\ell=1, m_\ell=0$) cases, since they may be the most relevant to current experiments involving ultracold atoms.

In Fig. 13, we show the evolution of $\mathcal{C}_{0,0}$ as a function of $1/(k_Fa_0)$ for the s-wave case. The weak-coupling Anderson-Bogoliubov velocity $\mathcal{C}_{0,0}=v_F/\sqrt{3}$ evolves continuously to the strong-coupling Bogoliubov velocity $\mathcal{C}_{0,0}=v_F\sqrt{k_Fa_0/(3\pi)}$. Notice that the sound velocity is a monotonically decreasing function of $1/(k_Fa_0)$, and the evolution across $\mu_0=0$ is a crossover.

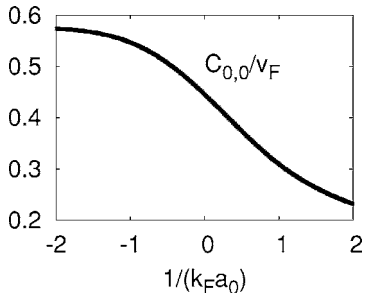

FIG. 13. Plots of reduced Goldstone (sound) velocity $(\mathcal{C}_{0,0})_r = \mathcal{C}_{0,0}/v_F$ vs interaction strength $1/(k_Fa_0)$ for $k_0 \approx 200k_F$.

In Fig. 14, we show the evolution of $\mathcal{C}^{i,j}_{1,0}$ as a function of $1/(k_F^3a_1)$ for the p-wave case. Notice that $\mathcal{C}^{i,i}_{1,0}$ is strongly anisotropic in weak coupling, since $\mathcal{C}^{x,x}_{1,0}=\mathcal{C}^{y,y}_{1,0} \approx 0.44v_F$ and $\mathcal{C}^{z,z}_{1,0}=\sqrt{3}\mathcal{C}^{x,x}_{1,0} \approx 0.79v_F$, thus reflecting the order-parameter symmetry. In addition, $\mathcal{C}^{i,i}_{1,0}$ is isotropic in strong coupling, since $\mathcal{C}^{i,i}_{1,0}=v_F\sqrt{3k_F/(2\pi k_0)} \approx 0.049v_F$ for $k_0 \approx 200k_F$, thus revealing the secondary role of the order-parameter symmetry in this limit. The anisotropy is very small in the intermediate regime beyond $\mu_1 < 0$. Notice also that $\mathcal{C}^{z,z}_{1,0}$ is a monotonically decreasing function of $1/(k_F^3a_1)$ in the BCS side until $\mu_1=0$, where it saturates. However, $\mathcal{C}^{x,x}_{1,0}=\mathcal{C}^{y,y}_{1,0}$ is a nonmonotonic function of $1/(k_Fa_1)^3$, and it also saturates beyond $\mu_1=0$. Therefore the behavior of $\mathcal{C}^{i,i}_{1,0}$ reflects the disappearance of nodes of the quasiparticle energy $E_1(\mathbf{k})$ as μ_1 changes sign.

These collective excitations may contribute significantly to the thermodynamic potential, which is discussed next.

E. Corrections to Ω^{sp}_ℓ due to collective modes

In this section, we analyze corrections to the saddle-point thermodynamic potential Ω^{sp}_ℓ due to low-energy collective excitations. The evaluation of Bosonic Matsubara frequency sums in Eq. (10) leads to $\Omega^{fluct}_\ell \to \Omega^{coll}_\ell$, where

$$\Omega^{coll}_\ell = \sum_{\mathbf{q}}{}' \left(W_\ell(\mathbf{q}) + \frac{2}{\beta}\ln\{1-\exp[-\beta W_\ell(\mathbf{q})]\}\right) \tag{62}$$

is the collective-mode contribution to the thermodynamic potential. The prime on the summation indicates that a momen-

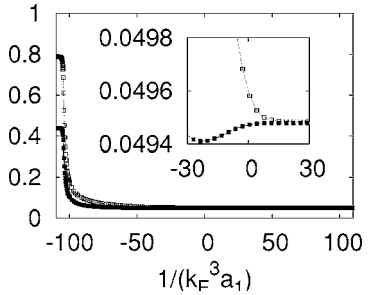

FIG. 14. Plots of reduced Goldstone (sound) velocity $(\mathcal{C}^{x,x}_{1,0})_r = \mathcal{C}^{x,x}_{1,0}/v_F$ (solid squares) and $(\mathcal{C}^{z,z}_{1,0})_r = \mathcal{C}^{z,z}_{1,0}/v_F$ (hollow squares) vs interaction strength $1/(k_F^3a_1)$ for $k_0 \approx 200k_F$. The inset zooms into the unitarity region.

tum cutoff is required since a long-wavelength and low-frequency approximation is used to derive the collective-mode dispersion. Notice that the first term in Eq. (62) contributes to the ground-state energy of the interacting Fermi system. This contribution is necessary to recover the ground-state energy of the effective Bose system in the strong-coupling limit.

The corrections to the saddle-point number equation $N_\ell^{\rm coll}=-\partial\Omega_\ell^{\rm coll}/\partial\mu_\ell$ are due to the zero-point motion ($N_\ell^{\rm zp}$) and thermal excitation ($N_\ell^{\rm te}$) of the collective modes,

$$N_\ell^{\rm zp}=-\frac{\partial}{\partial\mu_\ell}{\sum_{\mathbf{q}}}' W_\ell(\mathbf{q}), \tag{63}$$

$$N_\ell^{\rm te}=-{\sum_{\mathbf{q}}}'\frac{\partial W_\ell(\mathbf{q})}{\partial\mu_\ell}n_{\rm B}[W_\ell(\mathbf{q})]. \tag{64}$$

Here $n_{\rm B}(x)=1/[\exp(\beta x)-1]$ is the Bose distribution. For $\ell=0$, the last equation can be solved to obtain $N_0^{\rm te}=-6(\partial\mathcal{C}_{0,0}/\partial\mu_0)\zeta(4)T^4/(\pi^2\mathcal{C}_{0,0}^2)$, which vanishes at $T=0$. Here $\zeta(x)$ is the zeta function. Similarly, $N_{\ell\neq0}^{\rm te}$ has a power-law dependence on T, and therefore vanishes at $T=0$ since the collective modes are not excited. $N_\ell^{\rm zp}$ gives small contributions to the number equation in weak and strong couplings, but may lead to significant contributions in the intermediate regime for all ℓ. The impact of $N_\ell^{\rm zp}$ on the order parameter and chemical potential in the intermediate regime may require a careful analysis of the full fluctuation contributions [40].

Until now, we discussed the evolution of superfluidity from the BCS to the BEC regime at zero temperature. In the rest of the manuscript, we analyze the evolution of superfluidity from the BCS to the BEC limit at finite temperatures.

VI. BCS TO BEC EVOLUTION NEAR $T=T_{c,\ell}$

In this section, we concentrate on physical properties near critical temperatures $T=T_{c,\ell}$. To calculate $T_{c,\ell}$, the self-consistency (order-parameter and number) equations have to be solved simultaneously. At $T=T_{c,\ell}$, then $\Delta_{\ell,m_\ell}=0$, and the saddle-point order-parameter equation (19) reduces to

$$\frac{M\mathcal{V}}{4\pi k_0^{2\ell}a_\ell}=\sum_{\mathbf{k}}\Gamma_\ell^2(k)\left[\frac{1}{2\epsilon(\mathbf{k})}-\frac{\tanh[\xi_\ell(\mathbf{k})/(2T_{c,\ell})]}{2\xi_\ell(\mathbf{k})}\right]. \tag{65}$$

This expression is independent of m_ℓ since the interaction amplitude λ_ℓ depends only on ℓ. Similarly, the saddle point number equation reduces to

$$N_\ell^{\rm sp}=\sum_{\mathbf{k},s}n_{\rm F}[\xi_\ell(\mathbf{k})], \tag{66}$$

where $n_{\rm F}(x)=1/[\exp(\beta x)+1]$ is the Fermi distribution. Notice that the summation over spins (s) is not present in the SHS case. It is important to emphasize that the inclusion of $N_\ell^{\rm fluct}$ around $T_\ell=T_{c,\ell}$ is essential to produce the qualitatively correct physics with increasing coupling, as discussed next.

A. Gaussian fluctuations

To evaluate the Gaussian contribution to the thermodynamic potential, we sum over the Fermionic Matsubara Frequencies in Eq. (10), and obtain the action $S_\ell^{\rm fluct}=\beta\Sigma_{q,m_\ell,m_\ell'}\Lambda_{\ell,m_\ell}^\dagger(q)L_{\ell,m_\ell,m_\ell'}^{-1}(q)\Lambda_{\ell,m_\ell'}(q)$, where $L_{\ell,m_\ell,m_\ell'}^{-1}(q)=(\mathbf{F}_{\ell,m_\ell,m_\ell'}^{-1})_{11}$ is the element of the fluctuation propagator given by

$$L_{\ell,m_\ell,m_\ell'}^{-1}(q)=\frac{\delta_{m_\ell,m_\ell'}}{4\pi\mathcal{V}^{-1}\lambda_\ell}-\sum_{\mathbf{k}}\frac{1-n_{\rm F}(\xi_+)-n_{\rm F}(\xi_-)}{\xi_++\xi_--iv_j}$$

$$\Gamma_\ell^2(k)Y_{\ell,m_\ell}(\hat{\mathbf{k}})Y_{\ell,m_\ell'}^*(\hat{\mathbf{k}}). \tag{67}$$

This is the generalization of the $\ell=0$ case to $\ell\neq0$, where $\xi_\pm=\xi_\ell(\mathbf{k}\pm\mathbf{q}/2)$. From $S_\ell^{\rm fluct}$, we obtain the thermodynamic potential $\Omega_\ell^{\rm gauss}=\Omega_\ell^{\rm sp}+\Omega_\ell^{\rm fluct}$, where $\Omega_\ell^{\rm sp}$ is the saddle-point contribution with $\Delta_\ell(\mathbf{k})=0$, and $\Omega_\ell^{\rm fluct}=-\frac{1}{\beta}\Sigma_q\ln\det[L_\ell(q)/\beta]$ is the fluctuation contribution.

We evaluate the bosonic Matsubara frequency (iv_j) sums by using contour integration, and determine the branch cut and pole terms. We use the phase shift $\varphi_\ell^{\rm fluct}(\mathbf{q},w)=\mathrm{Arg}[\det L_\ell(\mathbf{q},iv_j\to w+i0^+)]$ to replace $\det L_\ell(q)$, leading to

$$\Omega_\ell^{\rm fluct}=-\sum_{\mathbf{q}}\int_{-\infty}^{\infty}\frac{dw}{\pi}n_{\rm B}(w)\tilde{\varphi}_\ell^{\rm fluct}(\mathbf{q},w), \tag{68}$$

where $\tilde{\varphi}_\ell^{\rm fluct}(\mathbf{q},w)=\varphi_\ell^{\rm fluct}(\mathbf{q},w)-\varphi_\ell^{\rm fluct}(\mathbf{q},0)$ and $n_{\rm B}(x)=1/[\exp(\beta x)-1]$ is the Bose distribution. Notice that this equation is the generalization of the s-wave ($\ell=0$) case [11,12] for $\ell\neq0$. Furthermore, the phase shift can be written as $\tilde{\varphi}_\ell^{\rm fluct}(\mathbf{q},w)=\tilde{\varphi}_\ell^{\rm sc}(\mathbf{q},w)+\tilde{\varphi}_\ell^{\rm bs}(\mathbf{q},w)$, where $\tilde{\varphi}_\ell^{\rm sc}(\mathbf{q},w)=\tilde{\varphi}_\ell(\mathbf{q},w)\Theta(w-w_{\mathbf{q}}^*)$, is the branch cut (scattering) and $\tilde{\varphi}_\ell^{\rm bs}(\mathbf{q},w)$ is the pole (bound state) contribution. Here, $\Theta(x)$ is the Heaviside function, $w_{\mathbf{q}}^*=w_{\mathbf{q}}-2\mu_\ell$ with $w_{\mathbf{q}}=|\mathbf{q}|^2/(4M)$ is the branch frequency and μ_ℓ is the Fermionic chemical potential.

The branch cut (scattering) contribution to the thermodynamic potential becomes $\Omega_\ell^{\rm sc}=-\Sigma_{\mathbf{q}}\int_{-\infty}^{\infty}\frac{dw}{\pi}n_{\rm B}(w)\tilde{\varphi}_\ell^{\rm sc}(\mathbf{q},w)$. For each $\mathbf{q}$, the integrand is nonvanishing only for $w>w_{\mathbf{q}}^*$ since $\tilde{\varphi}_\ell^{\rm sc}(\mathbf{q},w)=0$ otherwise. Thus the branch cut (scattering) contribution to the number equation $N_\ell^{\rm sc}=-\partial\Omega_\ell^{\rm sc}/\partial\mu_\ell$ is given by

$$N_\ell^{\rm sc}=\sum_{\mathbf{q}}\int_0^\infty\frac{dw}{\pi}\left[\frac{\partial n_{\rm B}(\tilde{w})}{\partial\mu_\ell}-n_{\rm B}(\tilde{w})\frac{\partial}{\partial\mu_\ell}\right]\tilde{\varphi}_\ell(\mathbf{q},\tilde{w}), \tag{69}$$

where $\tilde{w}=w+w_{\mathbf{q}}^*$.

When $a_\ell<0$, there are no bound states above $T_{c,\ell}$ and $N_\ell^{\rm sc}$ represents the correction due to scattering states. However, when $a_\ell>0$, there are bound states represented by poles at $w<w_{\mathbf{q}}^*$. The pole (bound-state) contribution to the number equation is

$$N_\ell^{\rm bs}=-\sum_{\mathbf{q}}n_{\rm B}[\mathcal{W}_\ell(\mathbf{q})]\eta_\ell[\mathbf{q},\mathcal{W}_\ell(\mathbf{q})], \tag{70}$$

where $\mathcal{W}_\ell(\mathbf{q})$ corresponds to the poles of $L_\ell^{-1}(q)$ and

$$\eta_\ell[\mathbf{q},\mathcal{W}_\ell(\mathbf{q})] = \mathrm{Res}\left\{\frac{\partial \det L_\ell^{-1}[\mathbf{q},\mathcal{W}_\ell(\mathbf{q})]/\partial\mu_\ell}{\det L_\ell^{-1}[\mathbf{q},\mathcal{W}_\ell(\mathbf{q})]}\right\} \quad (71)$$

is the residue. Heavy numerical calculations are necessary to find the poles as a function of $\mathbf{q}$ for all couplings. However, in sufficiently strong coupling, when $n_F(\xi_\pm) \ll 1$ in Eq. (67), the pole (bound-state) contribution can be evaluated analytically by eliminating λ_ℓ in favor of the two-body bound-state energy $\tilde{E}_{b,\ell}$ in vacuum. Notice that $\tilde{E}_{b,\ell}$ is related to the $E_{b,\ell}$ obtained from the T-matrix approach, where multiple scattering events are included. However, they become identical in the dilute limit.

A relation between λ_ℓ and $\tilde{E}_{b,\ell}$ can be obtained by solving the Schroedinger equation for two fermions interacting via a pairing potential $V(r)$. After Fourier transforming from real to momentum space, the Schroedinger equation for the pair wave function $\psi(\mathbf{k})$ is

$$2\epsilon(\mathbf{k})\psi(\mathbf{k}) + \frac{1}{\mathcal{V}}\sum_{\mathbf{k}'} V(\mathbf{k},\mathbf{k}')\psi(\mathbf{k}') = \tilde{E}_b\psi(\mathbf{k}). \quad (72)$$

Using the Fourier expansion of $V(\mathbf{k},\mathbf{k}')$ given in Eq. (2) and choosing only the ℓth angular momentum channel, we obtain

$$\frac{1}{\lambda_\ell} = \frac{1}{\mathcal{V}}\sum_{\mathbf{k}} \frac{\Gamma_\ell^2(k)}{2\epsilon(\mathbf{k}) - \tilde{E}_{b,\ell}}. \quad (73)$$

This expression relates $\tilde{E}_{b,\ell} < 0$ to λ_ℓ in order to express Eq. (74) in terms of binding energy $\tilde{E}_{b,\ell} < 0$. Notice that, this equation is similar to the order-parameter equation in the strong-coupling limit ($\mu_\ell < 0$ and $|\mu_\ell| \gg T_{c,\ell}$), where $\frac{1}{\lambda_\ell} = \frac{1}{\mathcal{V}}\Sigma_{\mathbf{k}}\frac{\Gamma_\ell^2(k)}{2\epsilon(\mathbf{k})-2\mu_\ell}$. Therefore $\mu_\ell \to \tilde{E}_{b,\ell}/2$ as the coupling increases.

Substitution of Eq. (73) in Eq. (71) yields the pole contribution which is given by $\mathcal{W}_\ell(\mathbf{q}) = w_\mathbf{q} + \tilde{E}_{b,\ell} - 2\mu_\ell$, and the residue at this pole is $\eta_\ell[\mathbf{q},\mathcal{W}_\ell(\mathbf{q})] = -2\Sigma_{m_\ell}$. Therefore the bound-state contribution to the phase shift in the sufficiently strong-coupling limit is given by $\tilde{\varphi}_\ell^{bs}(\mathbf{q},w) = \pi\Theta(w - w_\mathbf{q} + \mu_{B,\ell})$, which leads to the bound-state number equation

$$N_\ell^{bs} = 2\sum_{\mathbf{q},m_\ell} n_B[w_\mathbf{q} - \mu_{B,\ell}], \quad (74)$$

where $\mu_{B,\ell} = 2\mu_\ell - \tilde{E}_{b,\ell} \leq 0$ is the chemical potential of the Bosonic molecules. Notice that Eq. (74) is only valid for interaction strengths where $\mu_{B,\ell} \leq 0$. Thus this expression can not be used over a region of coupling strengths where $\mu_{B,\ell}$ is positive.

B. Critical temperature and chemical potential

To obtain the evolution from BCS to BEC, the number $N_\ell \approx N_\ell^{gauss} = N_\ell^{sp} + N_\ell^{sc} + N_\ell^{bs}$ and order-parameter [Eq. (65)] equations have to be solved self-consistently for $T_{c,\ell}$ and μ_ℓ. First, we analyze the number of unbound, scattering, and bound fermions as a function of the scattering parameter for the s-wave ($\ell = 0$) and p-wave ($\ell = 1$) cases.

In Fig. 15, we plot different contributions to the number equation as a function of $1/(k_F a_0)$ for the s-wave ($\ell = 0$, $m_\ell = 0$) case. Notice that N_0^{sp} (N_0^{bs}) dominates in weak (strong) coupling, while N_0^{sc} is the highest for intermediate couplings. Thus all fermions are unbound in the strictly BCS limit (not shown in the figure), while all fermions are bound in the strictly BEC limit.

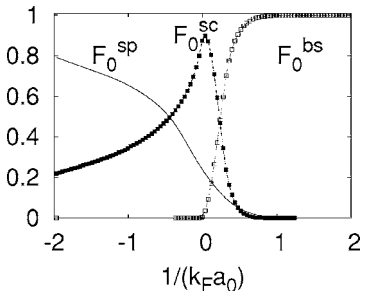

FIG. 15. Fractions of unbound $F_0^{sp} = N_0^{sp}/N_0$, scattering $F_0^{sc} = N_0^{sc}/N_0$, bound $F_0^{bs} = N_0^{bs}/N_0$ fermions at $T = T_{c,0}$ vs $1/(k_F a_0)$ for $k_0 \approx 200 k_F$.

In Fig. 16, we present plots of different contributions to the number equation as a function of $1/(k_F^3 a_1)$ for the p-wave ($\ell = 1$, $m_\ell = 0$) case. Notice also that N_1^{sp} (N_1^{bs}) dominates in weak (strong) coupling, while N_1^{sc} is the highest for intermediate couplings. Thus again all fermions are unbound in the strictly BCS limit, while all fermions are bound in the strictly BEC limit.

Therefore the total fluctuation contribution $N_\ell^{sc} + N_\ell^{bs}$ is negligible in weak coupling and N_ℓ^{sp} is sufficient. However, the inclusion of fluctuations is necessary for strong coupling to recover the physics of BEC. However, in the vicinity of the unitary limit $[1/(k_F^{2\ell+1} a_\ell) \to 0]$, our results are not strictly applicable and should be regarded as qualitative.

Next, we discuss the chemical potential and critical temperature. In weak coupling, we introduce a shell about the Fermi energy $|\xi_\ell(\mathbf{k})| \leq w_D$, such that $\mu_\ell \approx \epsilon_F \gg w_D \gg T_{c,\ell}$. Then, in Eq. (65), we set $\tanh[|\xi_\ell(\mathbf{k})|/(2T_{c,\ell})] = 1$ outside the shell and treat the integration within the shell as usual in the BCS theory. In strong coupling, we use that $\min[\xi_\ell(\mathbf{k})] = |\mu_\ell| \gg T_{c,\ell}$ and set $\tanh[\xi_\ell(\mathbf{k})/(2T_{c,\ell})] = 1$. Therefore, in strictly weak and strong coupling, the self-consistency equations are decoupled, and play reversed roles. In weak (strong) coupling the order-parameter equation determines $T_{c,\ell}$ (μ_ℓ) and the number equation determines μ_ℓ ($T_{c,\ell}$).

In weak coupling, the number equation $N_\ell \approx N_\ell^{sp}$ leads to

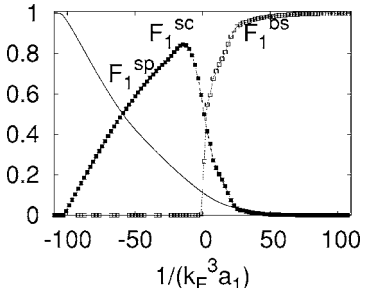

FIG. 16. Fractions of unbound $F_1^{sp} = N_1^{sp}/N_1$, scattering $F_1^{sc} = N_1^{sc}/N_1$, bound $F_1^{bs} = N_1^{bs}/N_1$ fermions at $T = T_{c,1}$ vs $1/(k_F^3 a_1)$ for $k_0 \approx 200 k_F$.

$$\mu_\ell \approx \epsilon_F \tag{75}$$

for any ℓ. In strong coupling, the order parameter equation leads to

$$\mu_0 = -\frac{1}{2Ma_0^2}, \tag{76}$$

$$\mu_{\ell\neq 0} = -\frac{\sqrt{\pi}}{Mk_0^{2\ell-1}a_\ell\phi_\ell}, \tag{77}$$

where $\phi_\ell=\Gamma(\ell-1/2)/\Gamma(\ell+1)$ and $\Gamma(x)$ is the Gamma function. This calculation requires $a_0k_0>1$ for $\ell=0$, and $k_0^{2\ell+1}a_\ell\phi_\ell>(\ell+1)\sqrt{\pi}$ for $\ell\neq 0$ for the order-parameter equation to have a solution with $\mu_\ell<0$. Furthermore, we assume $|\mu_\ell|\ll\epsilon_0=k_0^2/(2M)$ to obtain Eqs. (76) and (77). Notice that $\mu_\ell=E_{b,\ell}/2$ in this limit.

On the other hand, the solution of the order-parameter equation in weak coupling is

$$T_{c,0} = \frac{8}{\pi}\epsilon_F \exp\left[\gamma - 2 + \frac{\pi}{2}\frac{k_F}{k_0} - \frac{\pi}{2k_F|a_0|}\right], \tag{78}$$

$$T_{c,\ell} \sim \epsilon_F \exp\left[t_\ell\left(\frac{k_0}{k_F}\right)^{2\ell-1} - \frac{\pi}{2k_F^{2\ell+1}|a_\ell|}\right], \tag{79}$$

where $\gamma\approx 0.577$ is the Euler's constant, $t_1=\pi/4$ and $t_{\ell>1}=\pi 2^{\ell+1}(2\ell-3)!!/\ell!$. These expressions are valid only when the exponential terms are small. In strong coupling, the number equation $N_\ell\approx N_\ell^{bs}$ leads to

$$T_{c,\ell}^{THS} = \frac{2\pi}{M_{B,\ell}}\left[\frac{n_\ell}{\sum_{m_\ell}\zeta(3/2)}\right]^{2/3} = \frac{0.218}{\left(\sum_{m_\ell}\right)^{2/3}}\epsilon_F, \tag{80}$$

where $M_{B,\ell}=2M$ is the mass of the Bosonic molecules. Here, $n_\ell=k_F^3/(3\pi^2)$ is the density of fermions. For THS Fermi gases, we conclude that the BEC critical temperature of s-wave superfluids is the highest, and this temperature is reduced for higher angular momentum states. However, for SHS Fermi gases

$$T_{c,\ell\neq 0}^{SHS} = \frac{2\pi}{M_{B,\ell}}\left[\frac{n_\ell}{\sum_{m_\ell}\zeta(3/2)}\right]^{2/3} = \frac{0.137\epsilon_F}{\left(\sum_{m_\ell}\right)^{2/3}}, \tag{81}$$

where $n_\ell=k_F^3/(6\pi^2)$ and $\zeta(x)$ is the zeta function. Here, the summation over m_ℓ is over degenerate spherical harmonics involved in the order parameter of the system, and can be at most $\Sigma_{m_\ell}=2\ell+1$. For SHS states, we conclude that the BEC critical temperature of p-wave superfluids is the highest, and this temperature is reduced for higher angular momentum states.

For completeness, it is also possible to relate a_ℓ and $T_{c,\ell}$ when chemical potential vanishes. When $\mu_\ell=0$, the solution of number equation is highly nontrivial and it is difficult to find the value of the scattering parameter a_ℓ^* at $\mu_\ell=0$. However, the critical temperature in terms of a_ℓ^* can be found analytically from Eq. (65) as

$$\left(\frac{T_{c,\ell}}{\epsilon_F}\right)^{\ell+1/2} = \frac{\pi/(k_F^{2\ell+1}a_\ell^*)}{(2-2^{-\ell+3/2})\Gamma\left(\ell+\frac{1}{2}\right)\zeta\left(\ell+\frac{1}{2}\right)} \tag{82}$$

to order $T_{c,\ell}/\epsilon_0$, where $\epsilon_0=k_0^2/(2M)\gg T_{c,\ell}$. Notice that this relation depends on k_0 only through a_ℓ^*.

On the other hand, if temporal fluctuations are neglected, the solution for $T_{0,\ell}$ from the saddle-point self-consistency equations is $|\tilde{E}_{b,\ell}|=2T_{0,\ell}\ln[3\sqrt{\pi}(T_{0,\ell}/\epsilon_F)^{3/2}/4]$ and $\mu_\ell=\tilde{E}_{b,\ell}/2$ which leads to

$$T_{0,\ell} \sim \frac{|\tilde{E}_{b,\ell}|}{2\ln(|\tilde{E}_{b,\ell}|/\epsilon_F)^{3/2}} \tag{83}$$

up to logarithmic accuracy. Therefore $T_{0,\ell}$ grows without bound as the coupling increases. Within this calculation, the normal state for $T>T_{0,\ell}$ is described by unbound and nondegenerate fermions since $\Delta_\ell(\mathbf{k})=0$ and $|\mu_\ell|/T_{0,\ell}\sim\ln(|\tilde{E}_{b,\ell}|/\epsilon_F)^{3/2}\gg 1$. Notice that the saddle-point approximation becomes progressively worse with increasing coupling, since the formation of bound states is neglected.

We emphasize that there is no phase transition across $T_{0,\ell}$ in strong coupling. However, this temperature is related to the pair breaking or dissociation energy scale. To see this connection, we consider the chemical equilibrium between nondegenerate unbound fermions (f) and bound pairs (b) such that $b\leftrightarrow f\uparrow+f\downarrow$ for THS singlet states and $b\leftrightarrow f\uparrow+f\uparrow$ for SHS triplet states.

Notice that $T_{0,\ell}$ is sufficiently high that the chemical potential of the bosons and the fermions satisfy $|\mu_b|\gg T$ and $|\mu_f|\gg T$ at the temperature T of interest. Thus both the unbound fermions (f) and molecules (b) can be treated as classical ideal gases. The equilibrium condition $\mu_b=2\mu_f$ for these nondegenerate gases may be written as $T\ln\{n_b[2\pi/(M_bT)]^{3/2}\}-\tilde{E}_{b,\ell}=2T\ln\{n_f[2\pi/(M_fT)]^{3/2}\}$, where n_b (n_f) is the boson (fermion) density, M_b (M_f) is the boson (fermion) mass, and $\tilde{E}_{b,\ell}$ is the binding energy of a Bosonic molecule. The dissociation temperature above which some fraction of the bound pairs (molecules) are dissociated, is then found to be

$$T_{dissoc,\ell} \approx \frac{|\tilde{E}_{b,\ell}|}{\ln(|\tilde{E}_{b,\ell}|/\epsilon_F)^{3/2}}, \tag{84}$$

where we dropped a few constants of order unity. Therefore the logarithmic term is an entropic contribution which favors broken pairs and leads to a dissociation temperature considerably lower than the absolute value of binding energy $|\tilde{E}_{b,\ell}|$. The analysis above gives insight into the logarithmic factor appearing in Eq. (83) since $T_{0,\ell}\sim T_{dissoc,\ell}/2$. Thus $T_{0,\ell}$ is essentially the pair dissociation temperature of bound pairs (molecules), while $T_{c,\ell}$ is the phase coherence temperature corresponding to BEC of bound pairs (Bosonic molecules).

In Fig. 17, we show $T_{c,0}$ for the s-wave ($\ell=0$, $m_\ell=0$) case. Notice that $T_{c,0}$ grows from an exponential dependence in weak coupling to a constant in strong coupling with increasing interaction. Furthermore, the mean field $T_{0,0}$ and

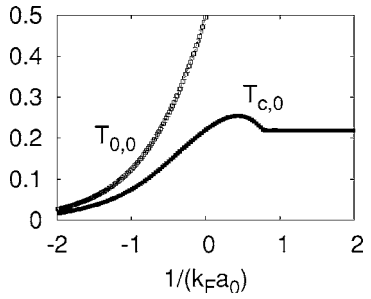

FIG. 17. Plot of reduced critical temperature $T_r=T_{c,0}/\epsilon_F$ vs interaction strength $1/(k_Fa_0)$ at $T=T_{c,0}$ for $k_0\approx 200k_F$.

Gaussian $T_{c,0}$ are similar only in weak coupling, while $T_{0,0}$ increases without bound as $T_{0,0}\sim 1/[(Ma_0^2)|\ln(k_Fa_0)|]$ in strong coupling. When $\mu_0=0$, we also obtain analytically $T_{c,0}/\epsilon_F\approx 2.15/(k_Fa_0^*)^2$ from Eq. (82). The hump in $T_{c,0}$ around $1/(k_Fa_0)\approx 0.5$ is similar to the those in Ref. [12], and might be an artifact of the approximations used here. Thus a more detailed self-consistent numerical analysis is needed to determine if this hump is real.

In Fig. 18, we show μ_0 for the s-wave case, where it changes from ϵ_F in weak coupling to $E_{b,0}/2=-1/(2Ma_0^2)$ in strong coupling. Notice that μ_0 at $T_{c,0}$ is qualitatively similar to μ_0 at $T=0$, however, it is reduced at $T_{c,0}$ in weak coupling. Furthermore, μ_0 changes sign at $1/(k_Fa_0)\approx 0.32$.

In Fig. 19, we show $T_{c,1}$ for the p-wave ($\ell=1$, $m_\ell=0$) case. $T_{c,1}$ grows from an exponential dependence in weak coupling to a constant in strong coupling with increasing interaction. For completeness, we present the limiting expressions $T_{c,1}=\frac{8}{\pi}\epsilon_F\exp\left[\gamma-\frac{8}{3}+\frac{\pi k_0}{4k_F}-\frac{\pi}{2k_F^3|a_1|}\right]$, and $T_{c,1}=\frac{2\pi}{M_{B,1}}\left[\frac{n_1}{\zeta(3/2)}\right]^{2/3}=0.137\epsilon_F$ in the weak- and strong-coupling limits, respectively. Furthermore, the mean field $T_{0,1}$ and Gaussian $T_{c,1}$ are similar only in weak coupling, while $T_{0,1}$ increases without bound as $T_{0,1}\sim 1/[(Mk_0a_1)|\ln(k_F^2k_0a_1)|]$ in strong coupling. When $\mu_1=0$, we also obtain analytically $T_{c,1}/\epsilon_F\approx 1.75/(k_F^3a_1^*)^{2/3}$ from Eq. (82). The hump in the intermediate regime is similar to the one found in fermion-boson model [36]. But to determine if this hump is real, it may be necessary to develop a fully self-consistent numerical calculation.

In Fig. 20, we show μ_1 for the p-wave case, where it changes from ϵ_F in weak coupling to $E_{b,1}/2=-1/(Mk_0a_1)$ in strong coupling. Notice that μ_1 at $T_{c,1}$ is both qualitatively and quantitatively similar to μ_1 at $T=0$. Furthermore, μ_1 changes sign at $1/(k_F^3a_1)\approx 0.02$.

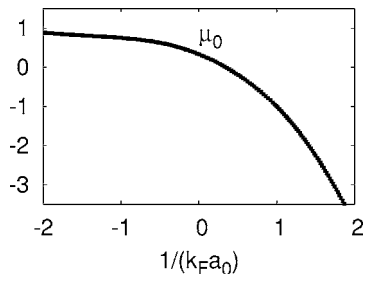

FIG. 18. Plot reduced chemical potential $\mu_r=\mu_0/\epsilon_F$ (inset) vs interaction strength $1/(k_Fa_0)$ at $T=T_{c,0}$ for $k_0\approx 200k_F$.

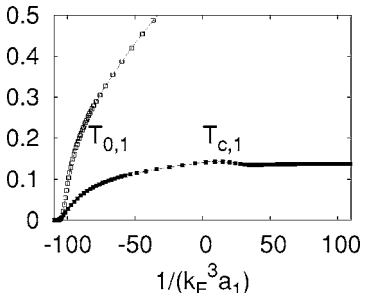

FIG. 19. Plot of reduced critical temperature $T_r=T_{c,1}/\epsilon_F$ vs interaction strength $1/(k_F^3a_1)$ at $T=T_{c,1}$ for $k_0\approx 200k_F$.

For any given ℓ, mean-field and Gaussian theories lead to similar results for $T_{c,\ell}$ and $T_{0,\ell}$ in the BCS regime, while they are very different in the BEC side. In the latter case, $T_{0,\ell}$ increases without bound, however, Gaussian theory results in a constant critical temperature which coincides with the BEC temperature of bosons. Notice that the pseudogap region $T_{c,\ell}<T<T_{0,\ell}$ for $\ell=0$ state is much larger than $\ell\neq 0$ states since $T_{0,\ell\neq 0}$ grows faster than $T_{0,\ell\neq 0}$. Furthermore, similar humps in $T_{c,\ell}$ around $1/(k_F^{2\ell+1}a_\ell)=0$ are expected for any ℓ as shown for the s-wave and p-wave cases, however, whether these humps are physical or not may require a fully self-consistent numerical approach.

As shown in this section, the frequency (temporal) dependence of fluctuations about the saddle point is crucial to describe adequately the Bosonic degrees of freedom that emerge with increasing coupling. In the next section, we derive the TDGL functional near $T_{c,\ell}$ to emphasize further the importance of these fluctuations.

VII. TDGL FUNCTIONAL NEAR $T_{c,\ell}$

Our basic motivation here is to investigate the low-frequency and long-wavelength behavior of the order parameter near $T_{c,\ell}$. To study the evolution of the time-dependent Ginzburg-Landau (TDGL) functional near $T_{c,\ell}$, we need to expand the effective action $S_\ell^{\rm eff}$ in Eq. (5) around $\Delta_{\ell,m_\ell}=0$ leading to

$$S_\ell^{\rm eff}=S_\ell^{\rm sp}+S_\ell^{\rm gauss}+\frac{\beta}{2}\sum_{\{q_n,m_{\ell_n}\}}b_{\ell,\{m_{\ell_n}\}}(\{q_n\})\Lambda^\dagger_{\ell,m_{\ell_1}}$$
$$\times(q_1)\Lambda_{\ell,m_{\ell_2}}(q_2)\Lambda^\dagger_{\ell,m_{\ell_3}}(q_3)\Lambda_{\ell,m_{\ell_4}}(q_1-q_2+q_3).$$

Here, $\Lambda_{\ell,m_\ell}(q)$ is the pairing fluctuation field.

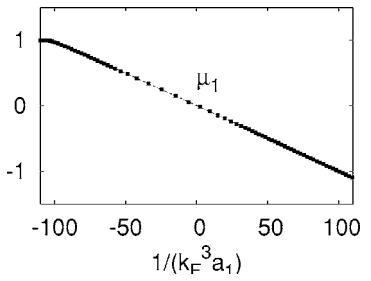

FIG. 20. Plot of reduced chemical potential $\mu_r=\mu_1/\epsilon_F$ (inset) vs interaction strength $1/(k_F^3a_1)$ at $T=T_{c,1}$ for $k_0\approx 200k_F$.

We first consider the static part of $L^{-1}_{\ell,m_\ell,m'_\ell}(q)$, and expand it in powers of q_i to get $L^{-1}_{\ell,m_\ell,m'_\ell}(\mathbf{q},0)=a_{\ell,m_\ell,m'_\ell}+\Sigma_{i,j}c^{i,j}_{\ell,m_\ell,m'_\ell}\frac{q_iq_j}{2M}+\cdots$. Next, we consider the time dependence of the TDGL equation, where it is necessary to expand $L^{-1}_{\ell,m_\ell,m'_\ell}(0,iv_j)-L^{-1}_{\ell,m_\ell,m'_\ell}(0,0)$ in powers of w after analytic continuation $iv_j\rightarrow w+i0^+$.

In the $x=(\mathbf{x},t)$ representation, the calculation above leads to the TDGL equation

$$\sum_{m_{\ell_2}}\left[a_{\ell,m_{\ell_1},m_{\ell_2}}-\sum_{i,j}c^{i,j}_{\ell,m_{\ell_1},m_{\ell_2}}\frac{\nabla_i\nabla_j}{2M}+\sum_{m_{\ell_3},m_{\ell_4}}b_{\ell,\{m_{\ell_n}\}}\times(0)\Lambda^{\dagger}_{\ell,m_{\ell_3}}(x)\Lambda_{\ell,m_{\ell_4}}(x)-id_{\ell,m_{\ell_1},m_{\ell_2}}\frac{\partial}{\partial t}\right]\Lambda_{\ell,m_{\ell_2}}(x)=0, \tag{85}$$

which is the generalization of the TDGL equation to higher momentum channels of THS singlet and SHS triplet states. Notice that, for THS triplet states, there may be extra gradient mixing textures and fourth-order terms in the expansion [39], which are not discussed here. All static and dynamic expansion coefficients are presented in Appendix B. The condition $\det a_\ell=0$ with matrix elements $a_{\ell,m_{\ell_1},m_{\ell_2}}$ is the Thouless criterion, which leads to the order-parameter equation. The coefficient $c^{i,j}_{\ell,m_{\ell_1},m_{\ell_2}}$ reflects a major difference between $\ell=0$ and $\ell\neq 0$ cases. While $c^{i,j}_{0,0,0}=c_{0,0,0}\delta_{i,j}$ is isotropic in space, $c^{i,j}_{\ell\neq 0,m_{\ell_1},m_{\ell_2}}$ is anisotropic, thus characterizing the anisotropy of the order parameter. The coefficient $b_{\ell,\{m_{\ell_n}\}}(0)$ is positive and guarantees the stability of the theory. The coefficient $d_{\ell,m_{\ell_1},m_{\ell_2}}$ is a complex number. Its imaginary part reflects the decay of Cooper pairs into the two-particle continuum for $\mu_\ell>0$. However, for $\mu_\ell<0$, imaginary part of $d_{\ell,m_{\ell_1},m_{\ell_2}}$ vanishes and the behavior of the order parameter is propagating reflecting the presence of stable bound states.

Next, we present the asymptotic forms of $a_{\ell,m_{\ell_1},m_{\ell_2}}$; $b_{\ell,\{m_{\ell_n}\}}(0)$; $c^{i,j}_{\ell,m_{\ell_1},m_{\ell_2}}$ and $d_{\ell,m_{\ell_1},m_{\ell_2}}$ which are used to recover the usual Ginzburg-Landau (GL) equation for BCS superfluids in weak coupling and the Gross-Pitaevskii (GP) equation for a weakly interacting dilute Bose gas in strong coupling.

A. Weak-coupling (BCS) regime

The weak-coupling BCS regime is characterized by $\mu_\ell>0$ and $\mu_\ell\approx\epsilon_F\gg T_{c,\ell}$. For any given ℓ, we find the following values for the coefficients:

$$a_{\ell,m_{\ell_1},m_{\ell_2}}=\kappa^{w}_\ell\ln\left(\frac{T}{T_{c,\ell}}\right)\delta_{m_{\ell_1},m_{\ell_2}}, \tag{86}$$

$$b_{\ell,\{m_{\ell_n}\}}(0)=7\gamma_{\ell,\{m_{\ell_n}\}}\frac{\kappa^{w}_\ell\zeta(3)}{8T^2_{c,\ell}}\left(\frac{\epsilon_F}{\epsilon_0}\right)^\ell, \tag{87}$$

$$c^{i,j}_{\ell,m_{\ell_1},m_{\ell_2}}=7\alpha^{i,j}_{\ell,m_{\ell_1},m_{\ell_2}}\frac{\kappa^{w}_\ell\epsilon_F\zeta(3)}{4\pi^2T^2_{c,\ell}}, \tag{88}$$

$$d_{\ell,m_{\ell_1},m_{\ell_2}}=\kappa^{w}_\ell\left(\frac{1}{4\epsilon_F}+i\frac{\pi}{8T_{c,\ell}}\right)\delta_{m_{\ell_1},m_{\ell_2}}, \tag{89}$$

where $\kappa^{w}_\ell=N(\epsilon_F)(\epsilon_F/\epsilon_0)^\ell/(4\pi)$ with $N(\epsilon_F)=M\mathcal{V}k_F/(2\pi^2)$ is the density of states per spin at the Fermi energy. Here $\delta_{m_{\ell_1},m_{\ell_2}}$ is the Kronecker delta, and $\alpha^{i,j}_{\ell,m_{\ell_1},m_{\ell_2}}$ and $\gamma_{\ell,\{m_\ell\}}$ are angular averaged quantities defined in Appendix B. Notice that the critical transition temperature is determined by $\det a_\ell=0$.

In the particular case, where only one of the spherical harmonics $Y_{\ell,m_\ell}(\hat{\mathbf{k}})$ is dominant and characterizes the order parameter, we can rescale the pairing field as

$$\Psi^{w}_{\ell,m_\ell}(x)=\sqrt{\frac{b_{\ell,\{m_\ell\}}(0)}{\kappa^{w}_\ell}}\Lambda_{\ell,m_\ell}(x) \tag{90}$$

to obtain the conventional TDGL equation

$$\left[-\varepsilon_\ell+|\Psi^{w}_{\ell,m_\ell}|^2-\sum_i(\xi^{GL}_{\ell,m_\ell})^2_i\nabla^2_i+\tau^{GL}_{\ell,m_\ell}\frac{\partial}{\partial t}\right]\Psi^{w}_{\ell,m_\ell}=0. \tag{91}$$

Here, $\varepsilon_\ell=(T_{c,\ell}-T)/T_{c,\ell}$ with $|\varepsilon_\ell|\ll 1$, $(\xi_{\ell,m_\ell})^2_i(T)=c^{i,i}_{\ell,m_\ell,m_\ell}/[2Ma_{\ell,m_\ell,m_\ell}]=(\xi^{GL}_{\ell,m_\ell})^2_i/\varepsilon_\ell$ is the characteristic GL length and $\tau_{\ell,m_\ell}=-id_{\ell,m_\ell,m_\ell}/a_{\ell,m_\ell,m_\ell}=\tau^{GL}_{\ell,m_\ell}/\varepsilon_\ell$ is the characteristic GL time.

In this limit, the GL coherence length is given by $k_F(\xi^{GL}_{\ell,m_\ell})_i=[7\alpha^{i,i}_{\ell,m_\ell,m_\ell}\zeta(3)/(4\pi^2)]^{1/2}(\epsilon_F/T_{c,\ell})$, which makes $(\xi^{GL}_{\ell,m_\ell})_i$ much larger than the interparticle spacing k_F^{-1}. There is a major difference between $\ell=0$ and $\ell\neq 0$ pairings regarding $(\xi^{GL}_{\ell,m_\ell})_i$. While $c^{i,j}_{0,0,0}=c_{0,0,0}\delta_{i,j}$ is isotropic, $c^{i,j}_{\ell\neq 0,m_{\ell_1},m_{\ell_2}}=c^{i,i}_{\ell,m_{\ell_1},m_{\ell_2}}\delta_{i,j}$ is in general anisotropic in space (see Appendix B). Thus $(\xi^{GL}_{0,0})_i$ is isotropic and $(\xi^{GL}_{\ell\neq 0,m_\ell})_i$ is not.

Furthermore, $\tau^{GL}_{\ell,m_\ell}=-i/(4\epsilon_F)+\pi/(8T_{c,\ell})$ showing that the dynamics of $\Psi^{w}_{\ell,m_\ell}(x)$ is overdamped reflecting the continuum of Fermionic excitations into which a pair can decay. In addition, there is a small propagating term since there is no perfect particle-hole symmetry. As the coupling grows, the coefficient of the propagating term increases while that of the damping term vanishes for $\mu_\ell\leqslant 0$. Thus the mode is propagating in strong coupling reflecting the stability of the bound states against the two particle continuum.

B. Strong-coupling (BEC) regime

The strong-coupling BEC regime is characterized by $\mu_\ell<0$ and $\epsilon_0=k_0^2/(2M)\gg|\mu_\ell|\gg T_{c,\ell}$. For $\ell=0$, we find the following coefficients:

$$a_{0,0,0}=2\kappa^{s}_0(2|\mu_0|-|\tilde{E}_{b,0}|), \tag{92}$$

$$b_{0,\{0\}}(0)=\frac{\kappa^{s}_0}{8\pi|\mu_0|}, \tag{93}$$

$$c^{i,j}_{0,0,0}=\kappa^{s}_0\delta_{i,j}, \tag{94}$$

$$d_{0,0,0} = 2\kappa_0^s, \tag{95}$$

where $\kappa_0^s = N(\epsilon_F)/(64\sqrt{\epsilon_F|\mu_0|})$. Similarly, for $\ell \neq 0$, we obtain

$$a_{\ell\neq 0,m_{\ell_1},m_{\ell_2}} = 2\kappa_\ell^s \phi_\ell(2|\mu_\ell| - |\tilde{E}_{b,\ell}|)\delta_{m_{\ell_1},m_{\ell_2}}, \tag{96}$$

$$b_{\ell\neq 0,\{m_{\ell_n}\}}(0) = 15\gamma_{\ell,\{m_{\ell_n}\}}\frac{\kappa_\ell^s \hat{\phi}_\ell}{2\epsilon_0}, \tag{97}$$

$$c^{i,j}_{\ell\neq 0,m_{\ell_1},m_{\ell_2}} = \kappa_\ell^s \phi_\ell \delta_{m_{\ell_1},m_{\ell_2}}\delta_{i,j}, \tag{98}$$

$$d_{\ell\neq 0,m_{\ell_1},m_{\ell_2}} = 2\kappa_\ell^s \phi_\ell \delta_{m_{\ell_1},m_{\ell_2}}, \tag{99}$$

where $\kappa_{\ell\neq 0}^s = N(\epsilon_F)/(64\sqrt{\pi\epsilon_F\epsilon_0})$. Here $\phi_\ell = \Gamma(\ell-1/2)/\Gamma(\ell+1)$ and $\hat{\phi}_\ell = \Gamma(2\ell-3/2)/\Gamma(2\ell+2)$, where $\Gamma(x)$ is the gamma function. Notice that $c^{i,j}_{\ell\neq 0,m_{\ell_1},m_{\ell_2}}$ is isotropic in space for any ℓ. Thus the anisotropy of the order parameter plays a secondary role in the TDGL theory in this limit.

In the particular case, where only one of the spherical harmonics $Y_{\ell,m_\ell}(\hat{\mathbf{k}})$ is dominant and characterizes the order parameter, we can rescale the pairing field as

$$\Psi^s_{\ell,m_\ell}(x) = \sqrt{d_{\ell,m_\ell,m_\ell}}\Lambda_{\ell,m_\ell}(x), \tag{100}$$

to obtain the conventional Gross-Pitaevskii (GP) equation

$$\left[\mu_{B,\ell} + U_{\ell,m_\ell}|\Psi^s_{\ell,m_\ell}|^2 - \frac{\nabla^2}{2M_{B,\ell}} - i\frac{\partial}{\partial t}\right]\Psi^s_{\ell,m_\ell} = 0 \tag{101}$$

for a dilute gas of bosons. Here, $\mu_{B,\ell} = -a_{\ell,m_\ell,m_\ell}/d_{\ell,m_\ell,m_\ell} = 2\mu_\ell - \tilde{E}_{b,\ell}$ is the chemical potential, $M_{B,\ell} = Md_{\ell,m_\ell,m_\ell}/c^{i,i}_{\ell,m_\ell,m_\ell} = 2M$ is the mass, and $U_{\ell,m_\ell} = b_{\ell,\{m_\ell\}}(0)/d^2_{\ell,m_\ell,m_\ell}$ is the repulsive interactions of the bosons. We obtain $U_{0,0} = 4\pi a_0/M$ and $U_{\ell\neq 0,m_\ell} = 240\pi^2\sqrt{\pi}\hat{\phi}_\ell\gamma_{\ell,\{m_\ell\}}/(M\phi_\ell^2 k_0)$ for $\ell = 0$ and $\ell \neq 0$, respectively. Notice that the mass of the composite bosons is independent of the anisotropy and symmetry of the order parameter for any given ℓ. However, this is not the case for the repulsive interactions between bosons, which explicitly depends on ℓ.

For $\ell = 0$, $U_{0,0} = 4\pi a_{B,0}/M_{B,0}$ is directly proportional to the fermion (boson) scattering length a_0 ($a_{B,0}$), where $a_{B,0} = 2a_0$ is the boson-boson scattering length. A better estimate for $a_{B,0} \approx 0.6a_0$ can be found in the literature [44–47]. While for $\ell \neq 0$, U_{ℓ,m_ℓ} is a constant (independent of the scattering parameter a_ℓ) depending only on the interaction range k_0 and the particular (ℓ, m_ℓ) state. For a finite range potential, $n_{B,\ell}U_{\ell,m_\ell}$ is small compared to ϵ_F, where $n_{B,\ell} = n_\ell/2$ is the density of bosons. In the $\ell = 0$ case $n_{B,0}U_{0,0}/\epsilon_F = 4k_F a_0/(3\pi)$ is much smaller than unity. For $\ell \neq 0$ and even, $n_{B,\ell}U_{\ell,m_\ell}/\epsilon_F = 80\sqrt{\pi}\hat{\phi}_\ell\gamma_{\ell,\{m_\ell\}}/\phi_\ell^2(k_F/k_0)$. In the case of SHS states where $\ell \neq 0$ and odd, $n_{B,\ell}U_{\ell,m_\ell}/\epsilon_F = 40\sqrt{\pi}\hat{\phi}_\ell\gamma_{\ell,\{m_\ell\}}/\phi_\ell^2(k_F/k_0)$. The results for higher angular momentum channels reflect the diluteness condition $(k_F/k_0)^3 \ll 1$.

To calculate $(\xi^{GL}_{\ell,m_\ell})_i$ in the strong-coupling limit, we need to know $\partial\mu_\ell/\partial T$ evaluated at $T_{c,\ell}$ (see below). The temperature dependence of μ_ℓ in the vicinity of $T_{c,\ell}$ can be obtained by noticing that $\mu_{B,\ell} = \tilde{n}(T)U_{\ell,m_\ell}$, where $\tilde{n}(T) = n_{B,\ell}[1 - (T/T_{c,\ell})^{3/2}]$. This leads to $k_F(\xi^{GL}_{\ell,m_\ell})_i = [\pi^2/(2Mk_F U_{\ell,m_\ell})]^{1/2}$ in the BEC regime. Using the asymptotic values of U_{ℓ,m_ℓ}, we obtain $k_F(\xi^{GL}_{0,0})_i = [\pi/(8k_F a_0)]^{1/2}$ for $\ell = 0$ and $k_F(\xi^{GL}_{\ell\neq 0,m_\ell})_i = [\phi_\ell^2/(480\sqrt{\pi}\gamma_{\ell,\{m_\ell\}}\hat{\phi}_\ell)]^{1/2}(k_0/k_F)^{1/2}$ for $\ell \neq 0$. Therefore $(\xi^{GL}_{\ell,m_\ell})_i$ is also much larger than the interparticle spacing k_F^{-1} in this limit, since $k_F a_0 \to 0$ for $\ell = 0$ and $k_0 \gg k_F$ for any ℓ.

C. Ginzburg-Landau coherence length versus average Cooper pair size

In the particular case, where only one of the spherical harmonics $Y_{\ell,m_\ell}(\hat{\mathbf{k}})$ is dominant and characterizes the order parameter, we can define the GL coherence length as $(\xi_{\ell,m_\ell})_i^2(T) = c^{i,i}_{\ell,m_\ell,m_\ell}/(2Ma_{\ell,m_\ell,m_\ell})$. An expansion of the parameters a_{ℓ,m_ℓ,m_ℓ} and $c^{i,i}_{\ell,m_\ell,m_\ell}$ in the vicinity of $T_{c,\ell}$ leads to $(\xi_{\ell,m_\ell})_i^2(T) \approx (\xi^{GL}_{\ell,m_\ell})_i^2\frac{T_{c,\ell}}{T_{c,\ell}-T}$, where the prefactor is the GL coherence length and given by

$$(\xi^{GL}_{\ell,m_\ell})_i^2 = \frac{c^{i,i}_{\ell,m_\ell,m_\ell}}{2MT_{c,\ell}}\left[\frac{\partial a_{\ell,m_\ell,m_\ell}}{\partial T}\right]^{-1}_{T=T_{c,\ell}}. \tag{102}$$

The slope of the coefficient a_{ℓ,m_ℓ,m_ℓ} with respect to T is given by $\frac{\partial a_{\ell,m_\ell,m_\ell}}{\partial T} = \Sigma_{\mathbf{k}}\left[\frac{\mathcal{Y}_\ell(\mathbf{k})}{2T^2} + \frac{\partial\mu_\ell}{\partial T}\left(\frac{\mathcal{Y}_\ell(\mathbf{k})}{2T\xi_\ell(\mathbf{k})} - \frac{\mathcal{X}_\ell(\mathbf{k})}{\xi_\ell^2(\mathbf{k})}\right)\right]\frac{\Gamma_\ell^2(k)}{8\pi}$. Here $\mathcal{X}_\ell(\mathbf{k})$ and $\mathcal{Y}_\ell(\mathbf{k})$ are defined in Appendix B. Notice that while $\partial\mu_\ell/\partial T$ vanishes at $T_{c,\ell}$ in weak coupling, it plays an important role in strong coupling. Furthermore, while $(\xi^{GL}_{\ell,m_\ell})_i$ representing the phase coherence length is large compared to interparticle spacing in both BCS and BEC limits, it should have a minimum near $\mu_\ell \approx 0$.

The prefactor $(\xi^{GL}_{\ell,m_\ell})_i$ of the GL coherence length must be compared with the average Cooper pair size ξ_ℓ^{pair} defined by

$$(\xi_\ell^{pair})^2 = \frac{\langle\mathcal{Z}_\ell(\mathbf{k})|r^2|\mathcal{Z}_\ell(\mathbf{k})\rangle}{\langle\mathcal{Z}_\ell(\mathbf{k})|\mathcal{Z}_\ell(\mathbf{k})\rangle} = -\frac{\langle\mathcal{Z}_\ell(\mathbf{k})|\nabla^2_{\mathbf{k}}|\mathcal{Z}_\ell(\mathbf{k})\rangle}{\langle\mathcal{Z}_\ell(\mathbf{k})|\mathcal{Z}_\ell(\mathbf{k})\rangle}, \tag{103}$$

where $\mathcal{Z}_\ell(\mathbf{k}) = \Delta_\ell(\mathbf{k})/[2E_\ell(\mathbf{k})]$ is the zero-temperature pair wave function. In the BCS limit, ξ_ℓ^{pair} is much larger than the interparticle distance k_F^{-1} since the Cooper pairs are weakly bound. Furthermore, for $\mu_\ell < 0$, we expect that ξ_ℓ^{pair} is a decreasing function of interaction for any ℓ, since Cooper pairs become more tightly bound as the interaction increases. Next, we compare $(\xi^{GL}_{\ell,m_\ell})_i$ and ξ_ℓ^{pair} for s-wave ($\ell = 0$) and p-wave ($\ell = 1$) states.

In Fig. 21, a comparison between $(\xi^{GL}_{0,0})_i$ and ξ_0^{pair} is shown for s-wave ($\ell = 0$, $m_\ell = 0$). ξ_0^{pair} changes from $k_F\xi_0^{pair} = [e^\gamma/\sqrt{2}\pi](\epsilon_F/T_{c,0})$ in the BCS limit to $k_F\xi_0^{pair} = [\epsilon_F/(2|\mu_0|)]^{1/2} = k_F a_0/\sqrt{2}$ in the BEC limit as the interaction

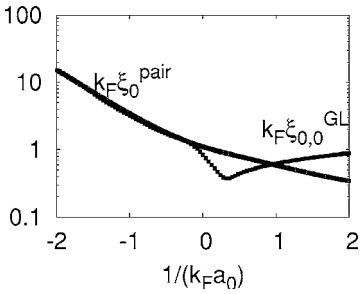

FIG. 21. Plots of GL coherence length $k_F\xi_{0,0}^{GL}$ (solid squares), and zero-temperature Cooper pair size $k_F\xi_{0,0}^{pair}$ (hollow squares) vs interaction strength $1/(k_Fa_0)$ at $T=T_{c,0}$ for $k_0\approx 200k_F$.

increases. Here $\gamma\approx 0.577$ is the Euler's constant. Furthermore, when $\mu_0=0$, we obtain $k_F\xi_0^{pair}=\sqrt{7}[\Gamma^2(1/4)/\sqrt{\pi}]^{1/3}/4\approx 1.29$, where $\Gamma(x)$ is the Gamma function. Notice that ξ_0^{pair} is continuous at $\mu_0=0$, and monotonically decreasing function of $1/(k_Fa_0)$ with a limiting value controlled by a_0 in strong coupling. However, $(\xi_{0,0}^{GL})_i$ is a nonmonotonic function of $1/(k_Fa_0)$ having a minimum around $1/(k_Fa_0)\approx 0.32$ ($\mu_0=0$). It changes from $k_F(\xi_{0,0}^{GL})_i=[7\zeta(3)/(12\pi^2)]^{1/2}(\epsilon_F/T_{c,0})$ in the BCS to $k_F(\xi_{0,0}^{GL})_i=[\pi/(8k_Fa_0)]^{1/2}$ in the BEC limit as the coupling increases, where $\zeta(x)$ is the Zeta function. Notice that, $(\xi_{0,0}^{GL})_i$ grows as $1/\sqrt{k_Fa_0}$ in strong-coupling limit.

In Fig. 22, a comparison between $(\xi_{1,0}^{GL})_z$ and ξ_1^{pair} is shown for p wave ($\ell=1$, $m_\ell=0$). Notice that, ξ_1^{pair} is nonanalytic at $\mu_1=0$, and is a monotonically decreasing function of $1/(k_F^3a_1)$ with a limiting value controlled by k_F/k_0 in strong coupling. This nonanalytic behavior is associated with the change in $E_1(\mathbf{k})$ from gapless (with line nodes) in the BCS to fully gapped in the BEC side. However, $(\xi_{1,0}^{GL})_z$ is a nonmonotonic function of $1/(k_F^3a_1)$ having a minimum around $1/(k_F^3a_1)\approx 0.02$ ($\mu_1=0$). It changes from $k_F(\xi_{1,0}^{GL})_x=k_F(\xi_{1,0}^{GL})_y=k_F(\xi_{1,0}^{GL})_z/\sqrt{3}=[7\zeta(3)/(20\pi^2)]^{1/2}(\epsilon_F/T_{c,1})$ in the BCS to $k_F(\xi_{1,0}^{GL})_i=[\pi k_0/(36k_F)]^{1/2}$ in the BEC limit as the coupling increases. Notice that, $\xi_{1,0}^{GL}$ saturates in strong-coupling limit reflecting the finite range of interactions.

It is important to emphasize that $(\xi_{\ell,m_\ell}^{GL})_z$ shown in Figs. (21) and (22) is only qualitative in the intermediate regime around unitarity $1/(k_F^{2\ell+1}a_\ell)=0$ since our theory is not strictly applicable in that region.

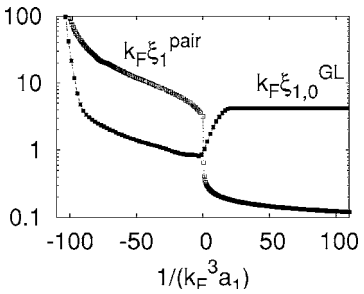

FIG. 22. Plots of GL coherence length $k_F\xi_{1,0}^{GL}$ (solid squares), and zero-temperature Cooper pair size $k_F\xi_{1,0}^{pair}$ (hollow squares) vs interaction strength $1/(k_F^3a_1)$ at $T=T_{c,1}$ for $k_0\approx 200k_F$.

VIII. CONCLUSIONS

In this manuscript, we extended the s-wave ($\ell=0$) functional integral formalism to finite angular momentum ℓ including two hyperfine states (THS) pseudospin singlet and single hyperfine states (SHS) pseudospin triplet channels. We analyzed analytically superfluid properties of a dilute Fermi gas in the ground state ($T=0$) and near critical temperatures ($T\approx T_{c,\ell}$) from weak coupling (BCS) to strong coupling (BEC) as a function of scattering parameter (a_ℓ) for arbitrary ℓ. However, we presented numerical results only for THS s-wave and SHS p-wave symmetries which may be relevant for current experiments involving atomic Fermi gases. The main results of our paper are as follows.

First, we analyzed the low-energy scattering amplitude within a T-matrix approach. We found that bound states occur only when $a_\ell>0$ for any ℓ. The energy of the bound states $E_{b,\ell}$ involves only the scattering parameter a_0 for $\ell=0$. However, another parameter related to the interaction range $1/k_0$ is necessary to characterize $E_{b,\ell}$ for $\ell\neq 0$. Therefore all superfluid properties for $\ell\neq 0$ depend strongly on k_0 and a_ℓ, while for $\ell=0$ they depend strongly only on a_0 but weakly on k_0.

Second, we discussed the order parameter, chemical potential, quasiparticle excitations, momentum distribution, atomic compressibility, ground-state energy, collective modes, and average Cooper pair size at $T=0$. There we showed that the evolution from BCS to BEC is just a crossover for $\ell=0$, while the same evolution for $\ell\neq 0$ exhibits a quantum phase transition characterized by a gapless superfluid on the BCS side to a fully gapped superfluid on the BEC side. This transition is a many body effect and takes place exactly when chemical potential $\mu_{\ell\neq 0}$ crosses the bottom of the fermion band ($\mu_{\ell\neq 0}=0$), and is best reflected as nonanalytic behavior in the ground-state atomic compressibility, momentum distribution, and average Cooper pair size.

Third, we discussed the critical temperature, chemical potential, and the number of unbound, scattering and bound fermions at $T=T_{c,\ell}$. We found that the critical BEC temperature is the highest for $\ell=0$. We also derived the time-dependent Ginzburg-Landau functional (TDGL) near $T_{c,\ell}$ and extracted the Ginzburg-Landau (GL) coherence length and time. We recovered the usual TDGL equation for BCS superfluids in the weak-coupling limit, whereas in the strong-coupling limit we recovered the Gross-Pitaevskii (GP) equation for a weakly interacting dilute Bose gas. The TDGL equation exhibits anisotropic coherence lengths for $\ell\neq 0$ which become isotropic only in the BEC limit, in sharp contrast to the $\ell=0$ case, where the coherence length is isotropic for all couplings. Furthermore, the GL time is a complex number with a larger imaginary component for $\mu_\ell>0$ reflecting the decay of Cooper pairs into the two-particle continuum. However, for $\mu_\ell<0$ the imaginary component vanishes and Cooper pairs become stable above $T_{c,\ell}$.

In summary, the BCS to BEC evolution in higher angular momentum ($\ell\neq 0$) states exhibit quantum phase transitions and is much richer than in conventional $\ell=0$ s-wave systems, where there is only a crossover. These $\ell\neq 0$ states might be found not only in atomic Fermi gases, but also in

nuclear (pairing in nuclei), astrophysics (neutron stars) and condensed-matter (high-T_c and organic superconductors) systems.

ACKNOWLEDGMENT

We would like to thank the NSF (Grant No. DMR-0304380) for financial support.

APPENDIX A: EXPANSION COEFFICIENTS AT $T=0$

From the rotated fluctuation matrix $\tilde{\mathbf{F}}_\ell^{-1}(q)$ expressed in the amplitude-phase basis, we can obtain the expansion coefficients necessary to calculate the collective modes at $T=0$. In the long-wavelength ($|\mathbf{q}|\to 0$) and low-frequency limit ($w\to 0$) the condition $\{w, \frac{q_i q_j}{2M}\} \ll \min\{2E_\ell(\mathbf{k})\}$ is used. While there is no Landau damping and a well defined expansion is possible for $\ell=0$ case for all couplings, extra care is necessary for $\ell\neq 0$ when $\mu_\ell>0$ since Landau damping is present.

In all the expressions below we use the following simplifying notation: $\dot{\xi}_\ell^i=\partial\xi_\ell(\mathbf{k}+\mathbf{q}/2)/\partial q_i$, $\ddot{\xi}_\ell^{i,j}=\partial\xi_\ell(\mathbf{k}+\mathbf{q}/2)/(\partial q_i\partial q_j)$, $\dot{\Delta}_\ell^i=\partial\Delta_\ell(\mathbf{k}+\mathbf{q}/2)/\partial q_i$, and $\ddot{\Delta}_\ell^{i,j}=\partial^2\Delta_\ell(\mathbf{k}+\mathbf{q}/2)/(\partial q_i\partial q_j)$, which are evaluated at $\mathbf{q}=0$.

The coefficients necessary to obtain the matrix element $(\tilde{\mathbf{F}}^{-1}_{\ell,m_\ell,m'_\ell})_{11}$ are

$$A_{\ell,m_\ell,m'_\ell}=\frac{\delta_{m_\ell,m'_\ell}}{4\pi\mathcal{V}^{-1}\lambda_\ell}-\sum_{\mathbf{k}}\frac{\xi_\ell^2}{2E_\ell^3}\Gamma_\ell^2(k)Y_{\ell,m_\ell}(\hat{\mathbf{k}})Y^*_{\ell,m'_\ell}(\hat{\mathbf{k}}), \tag{A1}$$

corresponding to the ($\mathbf{q}=0$, $w=0$) term,

$$\begin{aligned}C^{i,j}_{\ell,m_\ell,m'_\ell}=\sum_{\mathbf{k}}\frac{\xi_\ell(\mathbf{k})}{4E_\ell^7(\mathbf{k})}\{&\ddot{\xi}_\ell^{i,j}E_\ell^2(\mathbf{k})[\xi_\ell^2(\mathbf{k})-2\Delta_\ell^2(\mathbf{k})]\\&+3\ddot{\Delta}_\ell^{i,j}E_\ell^2(\mathbf{k})\xi_\ell(\mathbf{k})\Delta_\ell(\mathbf{k})+5\dot{\xi}_\ell^i\dot{\xi}_\ell^j\Delta_\ell^2(\mathbf{k})\xi_\ell^2(\mathbf{k})\\&+\dot{\Delta}_\ell^i\dot{\Delta}_\ell^j\xi_\ell(\mathbf{k})[\xi_\ell^2(\mathbf{k})-4\Delta_\ell^2(\mathbf{k})]+(\dot{\xi}_\ell^i\dot{\Delta}_\ell^j+\dot{\xi}_\ell^j\dot{\Delta}_\ell^i)\Delta_\ell(\mathbf{k})\\&\times[2\Delta_\ell^2(\mathbf{k})-3\xi_\ell^2(\mathbf{k})]\}\Gamma_\ell^2(k)Y_{\ell,m_\ell}(\hat{\mathbf{k}})Y^*_{\ell,m'_\ell}(\hat{\mathbf{k}}),\end{aligned} \tag{A2}$$

corresponding to the q_iq_j term, and

$$D_{\ell,m_\ell,m'_\ell}=\sum_{\mathbf{k}}\frac{\xi_\ell^2(\mathbf{k})}{8E_\ell^5(\mathbf{k})}\Gamma_\ell^2(k)Y_{\ell,m_\ell}(\hat{\mathbf{k}})Y^*_{\ell,m'_\ell}(\hat{\mathbf{k}}), \tag{A3}$$

corresponding to the w^2 term. Here δ_{m_ℓ,m'_ℓ} is the Kronecker delta.

The coefficients necessary to obtain the matrix element $(\tilde{\mathbf{F}}^{-1}_{\ell,m_\ell,m'_\ell})_{22}$ are

$$P_{\ell,m_\ell,m'_\ell}=\frac{\delta_{m_\ell,m'_\ell}}{4\pi\mathcal{V}^{-1}\lambda_\ell}-\sum_{\mathbf{k}}\frac{1}{2E_\ell(\mathbf{k})}\Gamma_\ell^2(k)Y_{\ell,m_\ell}(\hat{\mathbf{k}})Y^*_{\ell,m'_\ell}(\hat{\mathbf{k}}), \tag{A4}$$

corresponding to the ($\mathbf{q}=0$, $w=0$) term,

$$\begin{aligned}Q^{i,j}_{\ell,m_\ell,m'_\ell}=\sum_{\mathbf{k}}\frac{1}{4E_\ell^5(\mathbf{k})}\{&\ddot{\xi}_\ell^{i,j}E_\ell^2(\mathbf{k})\xi_\ell(\mathbf{k})+\ddot{\Delta}_\ell^{i,j}E_\ell^2(\mathbf{k})\Delta_\ell(\mathbf{k})\\&+3\dot{\xi}_\ell^i\dot{\xi}_\ell^j\Delta_\ell^2(\mathbf{k})+3\dot{\Delta}_\ell^i\dot{\Delta}_\ell^j\xi_\ell^2(\mathbf{k})-3(\dot{\xi}_\ell^i\dot{\Delta}_\ell^j\\&+\dot{\xi}_\ell^j\dot{\Delta}_\ell^i)\xi_\ell(\mathbf{k})\Delta_\ell(\mathbf{k})\}\Gamma_\ell^2(k)Y_{\ell,m_\ell}(\hat{\mathbf{k}})Y^*_{\ell,m'_\ell}(\hat{\mathbf{k}}),\end{aligned} \tag{A5}$$

corresponding to the q_iq_j term, and

$$R_{\ell,m_\ell,m'_\ell}=\sum_{\mathbf{k}}\frac{1}{8E_\ell^3(\mathbf{k})}\Gamma_\ell^2(k)Y_{\ell,m_\ell}(\hat{\mathbf{k}})Y^*_{\ell,m'_\ell}(\hat{\mathbf{k}}), \tag{A6}$$

corresponding to the w^2 term.

The coefficients necessary to obtain the matrix element $(\tilde{\mathbf{F}}^{-1}_{\ell,m_\ell,m'_\ell})_{12}$ is

$$B_{\ell,m_\ell,m'_\ell}=\sum_{\mathbf{k}}\frac{\xi_\ell(\mathbf{k})}{4E_\ell^3(\mathbf{k})}\Gamma_\ell^2(k)Y_{\ell,m_\ell}(\hat{\mathbf{k}})Y^*_{\ell,m'_\ell}(\hat{\mathbf{k}}), \tag{A7}$$

corresponding to the w term.

APPENDIX B: EXPANSION COEFFICIENTS AT $T=T_{c,\ell}$

In this section, we perform a small $\mathbf{q}$ and $iv_j\to w+i0^+$ expansion near $T_{c,\ell}$, where we assumed that the fluctuation field $\Lambda_{\ell,m_\ell}(\mathbf{x},t)$ is a slowly varying function of $\mathbf{x}$ and t.

The zeroth-order coefficient $L^{-1}_{\ell,m_\ell,m'_\ell}(0,0)$ is diagonal in m_ℓ and m'_ℓ, and is given by

$$a_{\ell,m_\ell,m'_\ell}=\frac{\delta_{m_\ell,m'_\ell}}{4\pi}\left[\frac{\mathcal{V}}{\lambda_\ell}-\sum_{\mathbf{k}}\frac{\mathcal{X}_\ell(\mathbf{k})}{2\xi_\ell(\mathbf{k})}\Gamma_\ell^2(k)\right], \tag{B1}$$

where $\mathcal{X}_\ell(\mathbf{k})=\tanh[\beta\xi_\ell(\mathbf{k})/2]$. The second-order coefficient $M\partial^2L^{-1}_{\ell,m_\ell,m'_\ell}(\mathbf{q},0)/(\partial q_i\partial q_j)$ evaluated at $\mathbf{q}=0$ is given by

$$\begin{aligned}c^{i,j}_{\ell,m_\ell,m'_\ell}=\frac{1}{4\pi}\sum_{\mathbf{k}}\Bigg\{&\left[\frac{\mathcal{X}_\ell(\mathbf{k})}{8\xi_\ell^2(\mathbf{k})}-\frac{\beta\mathcal{Y}_\ell(\mathbf{k})}{16\xi_\ell(\mathbf{k})}\right]\delta_{m_\ell,m'_\ell}\delta_{i,j}\\&+\alpha^{i,j}_{\ell,m_\ell,m'_\ell}\frac{\beta^2k^2\mathcal{X}_\ell(\mathbf{k})\mathcal{Y}_\ell(\mathbf{k})}{16M\xi_\ell(\mathbf{k})}\Bigg\}\Gamma_\ell^2(k),\end{aligned} \tag{B2}$$

where $\mathcal{Y}_\ell(\mathbf{k})=\mathrm{sech}^2[\beta\xi_\ell(\mathbf{k})/2]$ and the angular average

$$\alpha^{i,j}_{\ell,m_\ell,m'_\ell}=\int d\hat{\mathbf{k}}\hat{k}_i\hat{k}_jY_{\ell,m_\ell}(\hat{\mathbf{k}})Y^*_{\ell,m'_\ell}(\hat{\mathbf{k}}).$$

Here, $d\hat{\mathbf{k}}=\sin(\theta_\mathbf{k})d\theta_\mathbf{k}d\phi_\mathbf{k}$, $\hat{k}_x=\sin(\theta_\mathbf{k})\cos(\phi_\mathbf{k})$, $\hat{k}_y=\sin(\theta_\mathbf{k})\sin(\phi_\mathbf{k})$ and $\hat{k}_z=\cos(\theta_\mathbf{k})$. In general, $\alpha^{i,j}_{\ell,m_\ell,m'_\ell}$ is a fourth-order tensor for fixed ℓ. However, in the particular case where only one of the spherical harmonics $Y_{\ell,m_\ell}(\hat{\mathbf{k}})$ is dominant and characterizes the order parameter, $\alpha^{i,j}_{\ell,m_\ell,m'_\ell}=\alpha^{i,j}_{\ell,m_\ell,m_\ell}\delta_{m_\ell,m'_\ell}$ is diagonal in m_ℓ and m'_ℓ. In this case, we use Gaunt coefficients [48] to show that $\alpha^{i,j}_{\ell,m_\ell,m_\ell}$ is also diagonal in i and j leading to $\alpha^{i,j}_{\ell,m_\ell,m'_\ell}=\alpha^{i,i}_{\ell,m_\ell,m_\ell}\delta_{m_\ell,m'_\ell}\delta_{i,j}$.

The coefficient of fourth-order term is approximated at $q_n=0$, and given by

$$b_{\ell,\{m_{\ell_n}\}}(0)=\frac{\gamma_{\ell,\{m_{\ell_n}\}}}{4\pi}\sum_{\mathbf{k}}\left[\frac{\mathcal{X}_\ell(\mathbf{k})}{4\xi_\ell^3(\mathbf{k})}-\frac{\beta\mathcal{Y}_\ell(\mathbf{k})}{8\xi_\ell^2(\mathbf{k})}\right]\Gamma_\ell^4(k), \tag{B3}$$

where the angular average

$$\gamma_{\ell,\{m_{\ell_n}\}}=\int d\hat{\mathbf{k}}Y_{\ell,m_{\ell_1}}(\hat{\mathbf{k}})Y^*_{\ell,m_{\ell_2}}(\hat{\mathbf{k}})Y_{\ell,m_{\ell_3}}(\hat{\mathbf{k}})Y^*_{\ell,m_{\ell_4}}(\hat{\mathbf{k}}).$$

To extract the time dependence, we expand $Q_{\ell,m_\ell,m'_\ell}(iv_j)=L^{-1}_{\ell.m_\ell,m'_\ell}(\mathbf{q}=0,iv_j)-L^{-1}_{\ell,m_\ell,m'_\ell}(0,0)$ in powers of w after the analytic continuation $iv_j\to w+i0^+$. We use the relation $(x\pm i0^+)^{-1}=\mathcal{P}(1/x)\mp i\pi\delta(x)$, where $\mathcal{P}$ is the principal value and $\delta(x)$ is the delta function, to obtain

$$Q_{\ell,m_\ell,m'_\ell}(iv_j)=-\frac{\delta_{m_\ell,m'_\ell}}{4\pi}\left[\sum_{\mathbf{k}}\frac{\mathcal{X}_\ell(\mathbf{k})}{4\xi_\ell^2(\mathbf{k})}\Gamma_\ell^2(k)-i\pi\sum_{\mathbf{k}}\mathcal{X}_\ell(\mathbf{k})\delta[2\xi_\ell(\mathbf{k})-\mathbf{w}]\Gamma_\ell^2(\mathbf{k})\right]. \tag{B4}$$

Keeping only the first-order terms in w leads to $Q_{\ell,m_\ell,m'_\ell}(w+i0^+)=-d_{\ell,m_\ell,m'_\ell}w+\ldots$, where

$$d_{\ell,m_\ell,m'_\ell}=\frac{\delta_{m_\ell,m'_\ell}}{4\pi}\left[\sum_{\mathbf{k}}\frac{\mathcal{X}_\ell(\mathbf{k})}{4\xi_\ell^2(\mathbf{k})}\Gamma_\ell^2(k)+i\frac{\pi\beta}{8}N(\epsilon_F)\sqrt{\frac{\mu_\ell}{\epsilon_F}}\Gamma_\ell^2(\mu_\ell)\Theta(\mu_\ell)\right] \tag{B5}$$

is also diagonal in m_ℓ and m'_ℓ. Here $N(\epsilon_F)=M\mathcal{V}k_F/(2\pi^2)$ is the density of states per spin at the Fermi energy, $\Gamma_\ell^2(x)=(\epsilon_0x^\ell)/(\epsilon_0+x)^{\ell+1}$ is the interaction symmetry in terms of energy, and $\Theta(x)$ is the Heaviside function.

[1] C. A. Regal, M. Greiner, and D. S. Jin, Phys. Rev. Lett. **92**, 040403 (2004).
[2] M. Greiner, C. A. Regal, and D. S. Jin, Nature (London) **426**, 537 (2003).
[3] K. E. Strecker, G. B. Partridge, and R. G. Hulet, Phys. Rev. Lett. **91**, 080406 (2003).
[4] M. W. Zwierlein, C. A. Stan, C. H. Schunck, S. M. F. Raupach, S. Gupta, Z. Hadzibabic, and W. Ketterle, Phys. Rev. Lett. **91**, 250401 (2003).
[5] T. Bourdel, L. Khaykovich, J. Cubizolles, J. Zhang, F. Chevy, M. Teichmann, L. Tarruell, S. J. J. M. F. Kokkelmans, and C. Salomon, Phys. Rev. Lett. **93**, 050401 (2004).
[6] M. Bartenstein, A. Altmeyer, S. Riedl, S. Jochim, C. Chin, J. H. Denschlag, and R. Grimm, Phys. Rev. Lett. **92**, 120401 (2004).
[7] J. Kinast, S. L. Hemmer, M. E. Gehm, A. Turlapov, and J. E. Thomas, Phys. Rev. Lett. **92**, 150402 (2004).
[8] M. W. Zwierlein, J. R. Abo-Shaeer, A. Schirotzek, C. H. Schunck, and W. Ketterle, Nature (London) **435**, 1047 (2005).
[9] D. M. Eagles, Phys. Rev. **186**, 456 (1969).
[10] A. J. Leggett, in *Modern Trends in the Theory of Condensed Matter*, edited by A. Peralski and R. Przystawa (Springer-Verlag, Berlin, 1980).
[11] P. Nozieres and S. Schmitt-Rink, J. Low Temp. Phys. **59**, 195 (1985).
[12] C. A. R. Sá de Melo, M. Randeria, and J. R. Engelbrecht, Phys. Rev. Lett. **71**, 3202 (1993).
[13] J. R. Engelbrecht, M. Randeria, and C. A. R. Sá de Melo, Phys. Rev. B **55**, 15153 (1997).
[14] A. Perali, P. Pieri, L. Pisani, and G. C. Strinati, Phys. Rev. Lett. **92**, 220404 (2004).
[15] Y. Ohashi and A. Griffin, Phys. Rev. A **67**, 033603 (2003).
[16] M. Holland, S. J. J. M. F. Kokkelmans, M. L. Chiofalo, and R. Walser, Phys. Rev. Lett. **87**, 120406 (2001).
[17] E. Timmermans, K. Furuya, P. W. Milonni, and A. K. Kerman, Phys. Lett. A **285**, 228 (2001).
[18] Y. Ohashi and A. Griffin, Phys. Rev. Lett. **89**, 130402 (2002).
[19] C. A. Regal, C. Ticknor, J. L. Bohn, and D. S. Jin, Phys. Rev. Lett. **90**, 053201 (2003).
[20] C. Ticknor, C. A. Regal, D. S. Jin, and J. L. Bohn, Phys. Rev. A **69**, 042712 (2004)
[21] J. Zhang, E. G. M. van Kempen, T. Bourdel, L. Khaykovich, J. Cubizolles, F. Chevy, M. Teichmann, L. Tarruell, S. J. J. M. F. Kokkelmans, and C. Salomon, Phys. Rev. A **70**, 030702(R) (2004).
[22] C. H. Schunck, M. W. Zwierlein, C. A. Stan, S. M. F. Raupach, W. Ketterle, A. Simoni, E. Tiesinga, C. J. Williams, and P. S. Julienne, Phys. Rev. A **71**, 045601 (2005).
[23] K. Günter, T. Stöferle, H. Moritz, M. Köhl, and T. Esslinger, Phys. Rev. Lett. **95**, 230401 (2005).
[24] J. L. Bohn, Phys. Rev. A **61**, 053409 (2000).
[25] V. Gurarie, L. Radzihovsky, and A. V. Andreev, Phys. Rev. Lett. **94**, 230403 (2005).
[26] Chi-Ho Cheng and S.-K. Yip, Phys. Rev. Lett. **95**, 070404 (2005).
[27] L. S. Borkowski and C. A. R. Sá de Melo, e-print cond-mat/9810370.
[28] R. D. Duncan and C. A. R. Sá de Melo, Phys. Rev. B **62**, 9675 (2000).
[29] Jorge Quintanilla, Balazs L. Gyorffy, James F. Annett, and

Jonathan P. Wallington, Phys. Rev. B **66**, 214526 (2002).
[30] B. C. den Hertog, Phys. Rev. B **60**, 559 (1999).
[31] N. Andrenacci, A. Perali, P. Pieri, and G. C. Strinati, Phys. Rev. B **60**, 12410 (1999).
[32] Tin-Lun Ho and Roberto B. Diener, Phys. Rev. Lett. **94**, 090402 (2005).
[33] S. S. Botelho and C. A. R. Sá de Melo, e-print cond-mat/0409357
[34] M. Iskin and C. A. R. Sá de Melo, Phys. Rev. B **72**, 224513 (2005).
[35] S. S. Botelho and C. A. R. Sá de Melo, J. Low Temp. Phys. **140**, 409 (2005).
[36] Y. Ohashi, Phys. Rev. Lett. **94**, 050403 (2005).
[37] M. Iskin and C. A. R. Sá de Melo, Phys. Rev. Lett. **96**, 040402 (2006).
[38] L. D. Landau and E. M. Lifshitz, *Quantum Mechanics* (Permagon, Oxford, 1994).
[39] A. J. Leggett, Rev. Mod. Phys. **47**, 331 (1975).
[40] P. Pieri, L. Pisani, and G. C. Strinati, Phys. Rev. B **70**, 094508 (2004).
[41] M. Greiner, C. A. Regal, J. T. Stewart, and D. S. Jin, Phys. Rev. Lett. **94**, 110401 (2005).
[42] E. Altman, E. Demler, and M. D. Lukin, Phys. Rev. A **70**, 013603 (2004).
[43] F. Reif, *Fundamentals of Statistical and Thermal Physics* (McGraw-Hill, Tokyo, 1981), Chap. 8.
[44] P. Pieri and G. C. Strinati, Phys. Rev. B **61**, 15370 (2000).
[45] D. S. Petrov, C. Salomon, and G. V. Shlyapnikov, Phys. Rev. Lett. **93**, 090404 (2004).
[46] I. V. Brodsky, A. V. Klaptsov, M. Yu. Kagan, R. Combescot, and X. Leyronas, e-print cond-mat/0507240.
[47] J. Levinsen and V. Gurarie, e-print cond-mat/0510672.
[48] G. B. Arfken and H. J. Weber, *Mathematical Methods for Physicists* (Harcourt Academic Press, New York, 2001).